Broad-spectrum immune suppression encoded in self-amplifying RNA enables non-cytotoxic, non-immunostimulatory, externally controllable transgene expression

Tony K.Y Lim,[1,*] Anne Ritoux,[1] Luke W. Paine,[1] Larissa Ferguson,[2] Tawab Abdul,[1] and Ewan St. John Smith[1,**]

[1]Department of Pharmacology, University of Cambridge, Cambridge, UK

[2]MRC Laboratory of Molecular Biology, Cambridge, UK

*Correspondence: tony.ky.lim@gmail.com

**Correspondence: es336@cam.ac.uk

ABSTRACT

Self-amplifying RNA (saRNA) has the potential to provide durable, non-integrative transgene expression for transient gene therapy. However, its auto-replicative nature mimics viral infection, triggering innate immune responses that shutdown cap-dependent translation, degrade cellular mRNA, induce cell death, and release cytokines. In non-immunotherapy applications, this immune activation is undesirable as it limits transgene expression, depletes transfected cells, and induces inflammation, undermining therapeutic outcomes. Moreover, the use of exogenous immune suppressants to mitigate these effects often increases treatment complexity and the risk of unintended systemic side effects. To address these challenges, we developed a strategy to encode broad-spectrum innate immune suppression directly within saRNA. This approach leverages cap-independent translation to bypass saRNA-triggered translation shutdown, enabling the expression of multiple inhibitors targeting diverse double-stranded RNA-sensing and inflammatory signaling pathways. In mouse primary fibroblast-like synoviocytes—a cell type relevant to inflammatory joint diseases—this strategy eliminates the need for external immune inhibitors, reduces cytotoxicity and antiviral cytokine secretion, and enables sustained transgene expression that can be controlled with a small-molecule antiviral. These findings support the development of saRNA therapeutics that offer durable, non-integrative, externally controllable transgene expression without persistent immune activation or reliance on exogenous immune suppressants.

GRAPHICAL ABSTRACT

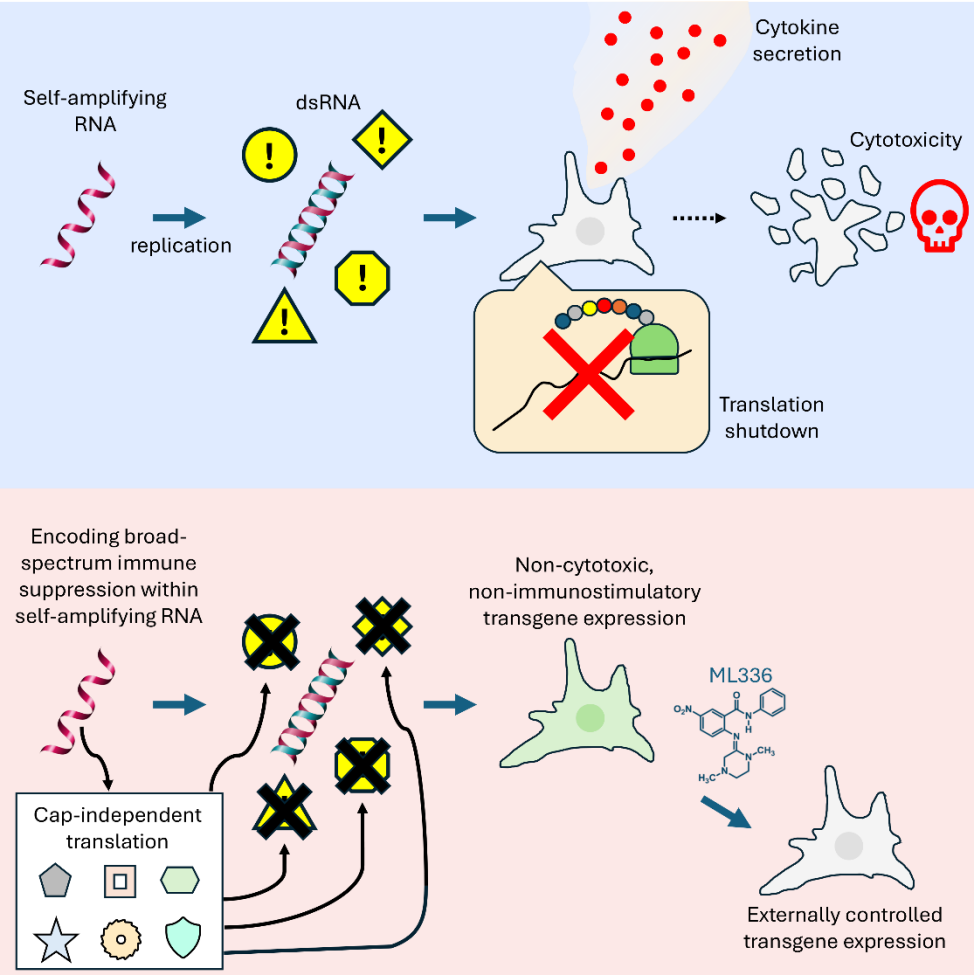

INTRODUCTION

Self-amplifying RNA (saRNA) is a promising platform for transient gene therapy due to its ability to encode large therapeutic payloads and achieve sustained, non-integrative protein expression.[1] Upon cellular internalization, saRNA utilizes host machinery to synthesize an RNA-dependent RNA polymerase (RdRp), which drives replication of the saRNA genome.[2] This process involves the production of a negative-strand RNA intermediate that serves as a template for both genomic and subgenomic RNA synthesis.[3] Subgenomic RNA, encoding the gene of interest, is transcribed in excess of the genomic RNA, leading to robust and sustained protein expression.[4]

However, the self-replication of saRNA also generates double-stranded RNA (dsRNA) intermediates, formed both during the synthesis of negative-strand RNA and during the transcription of positive-strand RNA from the negative-strand template.[3] These dsRNA intermediates are potent activators of cytosolic pattern recognition receptors, triggering innate immune responses.[5,6] This recognition results in shutdown of cap-dependent translation,[7–10] degradation of cellular mRNA,[6,11] induction of programmed cell death,[6,10,12–16] and release of cytokines and chemokines characteristic of viral infection.[9,17,18] In non-immunotherapy applications such as transient gene therapy, these responses are particularly problematic, as they limit transgene expression, deplete transfected cells, and induce inflammation.

Strategies to mitigate saRNA-mediated innate immune responses have included the incorporation of modified nucleotides[19], removal of dsRNA contaminants,[9,20] and co-delivery of non-replicating mRNA encoding viral innate immune inhibiting proteins.[21–23] While these approaches can reduce initial innate immune responses to saRNA transfection, they fall short in addressing the continuous immune activation triggered by dsRNA intermediates that arise during saRNA replication.[2] Sequence evolution of the RdRp replicon shows some promise in reducing these responses, but even engineered replicons still induce significant innate immune activation.[6,24] Encoding viral immune inhibitors within the saRNA construct using 2A self-cleaving peptides can improve protein expression *in vitro* but has limited impact on cytokine responses, despite reductions in NF-κB and IRF3 activation.[18] Although these strategies temper saRNA-induced innate immune responses to levels appropriate for immunotherapy applications—where some immune activation is beneficial[25]—they fall short of the stringent requirements for non-immunotherapy contexts, where therapeutic outcomes can be compromised by immune activation. In such cases, exogenous immunosuppressants can mitigate saRNA-induced immune responses and enable effective transgene expression,[9,21,26,27] but this approach complicates treatment regimens and increases the risk of unintended side effects from systemic immune suppression.

To address these challenges, we developed a fully saRNA-based approach that mitigates innate immune responses triggered by saRNA replication, incorporating several key innovations. First, innate immune inhibitory proteins are expressed via cap-independent translation, bypassing the cap-dependent translation shutdown commonly triggered by saRNA. Cap-dependent translation requires the presence of a 5′ cap structure on mRNA, which recruits translation initiation factors and ribosomes.[28] By contrast, cap-independent translation uses internal ribosome entry sites (IRES)—to recruit ribosomes directly to the mRNA, enabling translation even when cap-dependent pathways are inhibited.[29] Second, by simultaneously targeting multiple dsRNA-sensing and inflammatory signaling pathways, our method provides a more comprehensive suppression of innate immune responses than single target approaches. Third, encoding innate immune inhibitors directly within the saRNA ensures continuous protection against persistent innate immune activation caused by dsRNA intermediates during saRNA replication, eliminating the need for exogenous immunosuppressants.

We evaluated this approach in mouse primary fibroblast-like synoviocytes (FLS), a key cell type in the pathology of inflammatory joint diseases.[30,31] To facilitate this evaluation, we developed a microplate assay for straightforward, longitudinal monitoring of saRNA translation control and cytotoxicity in live cells. Our results demonstrate that this strategy effectively reduces saRNA-induced cytotoxicity and cytokine production while enabling sustained cap-dependent transgene expression, which can be reversed with a small-molecule antiviral. These results pave the way for saRNA-based therapies that offer durable, externally controllable transgene expression with minimal innate immune activation, achieving this without reliance on exogenous immunosuppressants.

RESULTS

Development of a microplate assay for longitudinal monitoring of translational control and cell number

Since saRNA can induce cap-dependent translation shutdown and cell death, we developed a microplate assay to simultaneously monitor cap-independent translation, cap-dependent translation, and cell number over time. In this assay, primary mouse FLS (Fig. S1) were plated in 6-well plates and transfected with saRNA constructs that used the Venezuelan equine encephalitis virus (VEEV) RdRp to self-replicate. These constructs featured a dual-fluorescence design, with EGFP expressed through encephalomyocarditis virus (EMCV) IRES-mediated, cap-independent translation, and mScarlet3 expressed through subgenomic cap-dependent translation. This dual-reporter system enabled

assessment of the effects of saRNA on translational control (Fig. 1a). Spectral overlap between EGFP and mScarlet3 was corrected using linear unmixing (Figs. S2a-c).

To monitor cell number, FLS were stained with BioTracker NIR680, a lipophilic carbocyanine membrane dye that enables long-term fluorescent labeling of cells.[32] Carbocyanine dyes like BioTracker are weakly fluorescent in aqueous solution but exhibit high fluorescence when integrated into lipid bilayers. Consequently, mock transfection with Lipofectamine MessengerMAX—a lipid transfection agent—enhanced BioTracker fluorescence compared to non-transfected cells, likely due to an interaction with the lipid components of Lipofectamine (Figs. S3a, S3b). Despite this interaction, BioTracker remains effective for indicating cell number, as treatment of mock transfected cells with the apoptosis inducer staurosporine[33] reduced BioTracker fluorescence (Figs. S3a, S3b). The BioTracker results were consistent with those obtained using the viability dye calcein AM (Figs. S3c, S3d), with the added advantages of eliminating the need for additional staining and wash steps and avoiding spectral overlap with red and green fluorescent proteins. This assay allows for seamless longitudinal monitoring of cap-independent translation, cap-dependent translation, and cell number using microplate readers or imagers.

Design of saRNA constructs for inhibiting multiple dsRNA sensing pathways

Cells detect cytosolic dsRNA through several sensing pathways, including RIG-I,[34] melanoma differentiation-associated protein 5 (MDA-5),[35] protein kinase R (PKR),[36] and the oligoadenylate synthase (OAS)/RNase L pathway.[37] To broadly inhibit these pathways, we designed an saRNA construct, referred to as ‘E3’, that utilizes EMCV IRES cap-independent translation to express the vaccinia virus E3 protein (Fig. 1a). E3 protein is a pleiotropic inhibitor that binds and sequesters dsRNA, effectively blocking multiple dsRNA sensing pathways.[38]

Given the key roles of PKR in cap-dependent translation shutdown and OAS/RNase L in cellular mRNA degradation in response to dsRNA, we sought to further inhibit these pathways in a second construct. This construct includes Toscana virus NSs, a ubiquitin ligase that promotes PKR degradation,[39] and Theiler’s virus L*, which inhibits RNase L.[40] To enable co-expression of these three proteins—E3, NSs, and L*—we incorporated 2A “self-cleaving” peptide sequences between the proteins, allowing the polyprotein to be cleaved into separate proteins during translation. As prior experiments showed that using multiple identical 2A peptides can reduce protein expression,[41] we selected non-identical 2A peptides for this construct. This construct, named ‘E3-NSs-L*’, is expected to provide a more comprehensive inhibition of dsRNA-sensing pathways than the E3 construct.

Finally, as a control, we designed a ‘native saRNA’ construct that expresses a blue fluorescent protein (moxBFP) as a visual marker of IRES functionality in place of inhibitors of dsRNA-sensing pathways. Importantly, moxBFP expression did not overlap spectrally with the EGFP or mScarlet3 channels (Figs. S2a-c).

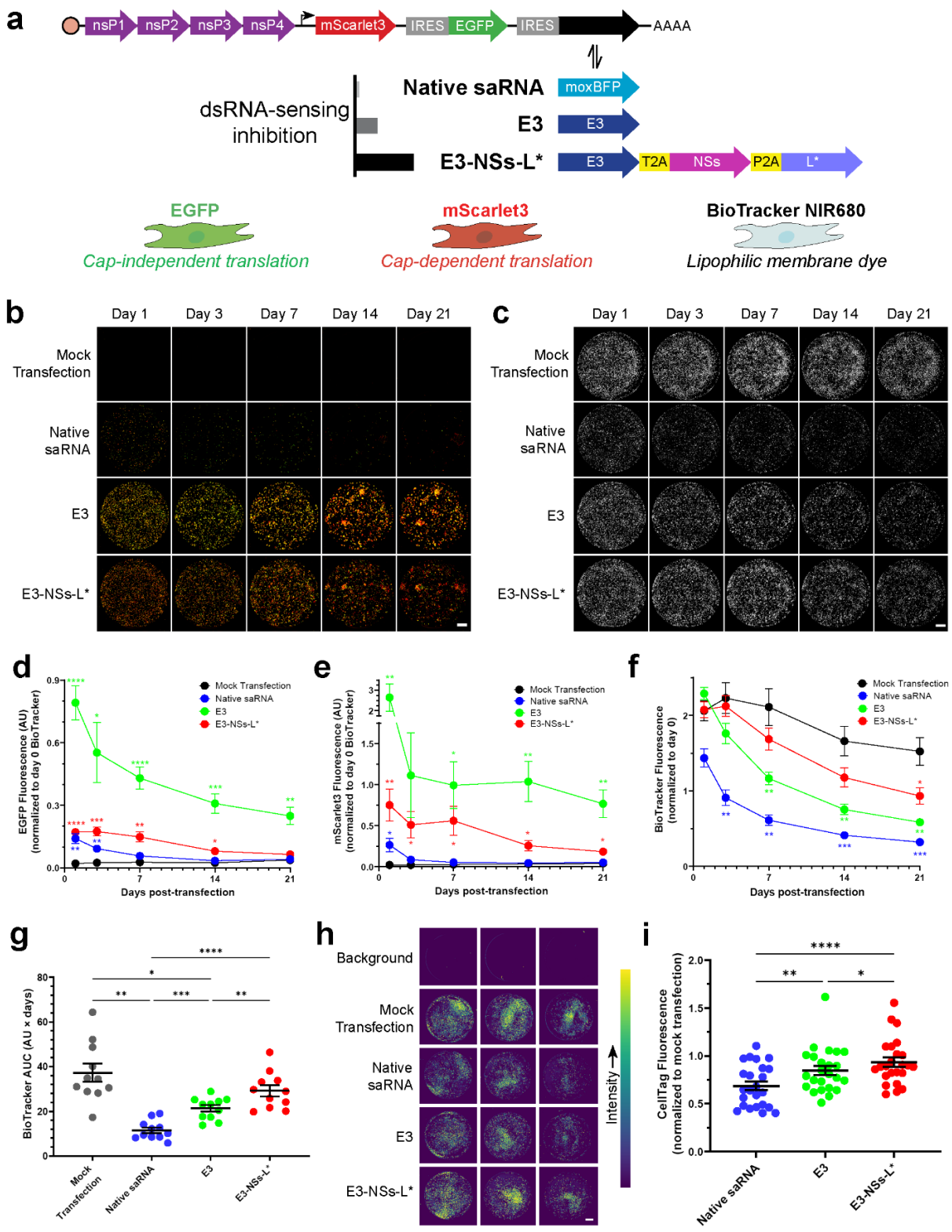

Fig. 1. Differential effects of moderate and strong dsRNA-sensing pathway inhibition on saRNA transgene expression and cell loss

a, Schematic of the native saRNA, E3, and E3-NSs-L* constructs designed to inhibit dsRNA-sensing pathways and report saRNA transgene expression. The native saRNA construct lacks dsRNA-sensing inhibitors. The E3 construct expresses vaccinia virus E3, a pleiotropic inhibitor of dsRNA sensing, expected to provide moderate inhibition. The E3-NSs-L* construct expresses vaccinia virus E3, and additionally includes Toscana virus NSs and Theiler's virus L*, which target the PKR and OAS/RNase L pathways, expected to provide strong inhibition. EGFP is expressed via an IRES to report cap-independent translation, while a subgenomic promoter (depicted with an angled arrow) enables transcription of an RNA transcript that expresses mScarlet3 via cap-dependent translation. saRNA constructs were transfected into primary mouse FLS, which were labeled with BioTracker to monitor cell number.

b, Representative images of EGFP (green) and mScarlet3 (red) expression in FLS transfected with native saRNA, E3, or E3-NSs-L* over 3 weeks. Scale bar = 5 mm.

c, Representative images of FLS transfected with the same constructs, showing BioTracker intensity over time. Scale bar = 5 mm.

d, Quantification of EGFP fluorescence over time (n = 11 biological replicates). The E3 construct provided the greatest EGFP expression, while the E3-NSs-L* construct showed intermediate levels. Statistical significance of treatment effects at each time point compared to mock transfection was determined by two-way RM ANOVA with Greenhouse–Geisser correction and Dunnett's multiple comparisons test.

e, Quantification of mScarlet3 fluorescence over time (n = 11 biological replicates). The E3 construct provided the greatest mScarlet3 expression, while the E3-NSs-L* showed intermediate levels. Statistical significance of treatment effects at each time point compared to mock transfection was determined by two-way RM ANOVA with Greenhouse–Geisser correction and Dunnett's multiple comparisons test.

f, Quantification of BioTracker fluorescence over time (n = 11 biological replicates). The native saRNA and E3 constructs reduced BioTracker fluorescence, indicating cell loss. Statistical significance of treatment effects at each time point compared to mock transfection was determined by two-way RM ANOVA with Greenhouse–Geisser correction and Dunnett's multiple comparisons test.

g, AUC analysis of BioTracker fluorescence data shown in (f), summarizing cumulative effects over the time course (n = 11 biological replicates). Increasing dsRNA-sensing pathway inhibition prevents saRNA-induced reductions in integrated BioTracker signal. Statistical analysis was performed using one-way RM ANOVA with Greenhouse–Geisser correction and Tukey's multiple comparisons test to compare all groups. Mock transfection data is also presented in Fig. S5a.

h, Representative images of FLS stained with the cell number normalization dye, CellTag 700. Columns represent cells plated from the same biological replicate, while rows show different treatments. Scale bar = 2.5 mm.

i, Quantification of mock transfection normalized CellTag signal (n = 24 biological replicates). Increasing dsRNA-sensing pathway inhibition mitigates saRNA-induced reductions in CellTag signal. Statistical analysis was performed using one-way RM ANOVA with Greenhouse–Geisser correction and Holm-Šídák's multiple comparisons test to compare all groups. Assays were performed 2 days post-transfection. Data in this panel were pooled from in-cell western assays, incorporating data presented in Figs. 3 and 6 as well as additional data not shown elsewhere.

For all statistical reporting, *$P < 0.05$, **$P < 0.01$, ***$P < 0.001$ and ****$P < 0.0001$. Data are presented as mean ± SEM.

For panels (d-f): Data were normalized to starting cell number, indicated by BioTracker intensity on day 0, prior to transfection. The mock transfection control data is also presented in Figs. 5c-e.

Acronyms: saRNA, self-amplifying RNA; dsRNA, double-stranded RNA; nsP, Venezuelan equine encephalitis virus non-structural protein; IRES, encephalomyocarditis virus internal ribosome entry site; moxBFP, monomeric oxidizing environment-optimized blue fluorescent protein; E3, Vaccinia virus E3 protein; NSs, Toscana virus non-structural NSs protein; L*, Theiler's murine encephalomyelitis virus L*

protein; T2A, Thosea asigna virus 2A peptide; P2A, porcine teschovirus-1 2A peptide; PKR, protein kinase R; OAS, oligoadenylate synthase; AUC, area under the curve.

Moderate dsRNA-sensing pathway inhibition enables high transgene expression at the cost of cell loss, while strong inhibition preserves cell number at lower expression levels

Following transfection of saRNA constructs, we monitored BioTracker, EGFP, and mScarlet3 fluorescence over 3 weeks (Figs. 1b, 1c). Inhibiting dsRNA-sensing pathways with viral proteins significantly enhanced saRNA transgene expression (Figs. 1d, 1e). Interestingly, the E3 construct produced the highest levels of EGFP and mScarlet3 expression, surpassing both native saRNA and the E3-NSs-L* construct. Native saRNA yielded low levels of transgene expression, while E3-NSs-L* showed intermediate expression.

Achieving durable transgene expression depends equally on preserving cell viability and maximizing transgene expression, as constructs that induce cell death undermine the goal of sustained transgene expression. Transfection of FLS with native saRNA caused both immediate and long-term reductions in cell number, as indicated by BioTracker intensity (Fig. 1f). While the E3 construct initially maintained cell number, BioTracker signals gradually diminished over time. In contrast, the E3-NSs-L* construct provided sustained protection against the decline in cell number. To quantify the cumulative effects of different saRNA constructs on cell number over the experimental time course, we performed area under the curve (AUC) analysis, demonstrating that E3-NSs-L* significantly protected against a decline in cell number compared to the E3 construct (Fig. 1g). These findings were further supported by experiments using CellTag, a cell number normalization stain (Fig. 1h), which revealed that increasing dsRNA-sensing pathway inhibition protects against cell loss (Fig. 1i). Together, these results suggest that while the E3 construct effectively enhances saRNA transgene expression, it is associated with greater cell loss, underscoring the advantage of the E3-NSs-L* construct for applications requiring sustained, non-cytotoxic gene expression.

Inhibiting dsRNA sensing pathways reduces saRNA-induced cytotoxicity and improves cell viability

saRNA is known to induce programmed cell death,[6,10,12–16] which often leads to cell detachment.[42] Thus reductions in BioTracker signal following saRNA treatment are likely indicative of this process. However, since BioTracker is a lipophilic membrane dye, the reduction in signal may not necessarily correlate with cell viability or cytotoxicity. In addition to long-term cell tracking, lipophilic membrane dyes like BioTracker are often used to stain extracellular vesicles, which bud off from the plasma membrane.[43] During cellular stress, increased production of extracellular vesicles[44] could deplete the membrane-associated BioTracker dye from cells, resulting in a lower detectable signal. Therefore, the observed reduction in BioTracker signal could reflect enhanced extracellular vesicle production rather than cell death.

To provide more definitive evidence that inhibiting dsRNA-sensing pathways protects against saRNA-induced cytotoxicity, we conducted a longitudinal assay with annexin V staining over 6 days (Fig. 2a), followed by calcein AM staining on day 7 (Fig. 2b). Annexin V, a membrane-impermeable protein, binds to phosphatidylserine, which translocates to the extracellular side of the cell membrane during early apoptosis, enabling the detection of apoptotic cells with intact membranes.[45] If the membrane is compromised, annexin V can enter cells and stain intracellular phosphatidylserine, indicating late apoptosis or necrosis.[46] Calcein AM, a viability dye, accumulates in metabolically active cells with intact membranes, serving both as a marker of live cell number and an indicator of membrane integrity.[47]

The apoptosis inducing agent staurosporine caused a transient increase in annexin V staining that decreased after the first day (Fig. 2c), along with a marked reduction in calcein AM fluorescence compared to mock transfection (Fig. 2d), observations that are consistent with extracellular

phosphatidylserine translocation and/or increased membrane permeability. Similarly, native saRNA induced a temporary increase in annexin V staining during the first two days post-transfection (Fig. 2c) accompanied by reduced calcein AM staining (Fig. 2d). Co-expression of E3 prevented the initial increase in annexin V staining, but elevated it from day 2 onward, and also resulted in significantly reduced calcein AM intensity (Figs. 2c, 2d). In contrast, E3-NSs-L* had no significant effect on annexin V or calcein AM staining compared to mock transfection, supporting the idea that broader inhibition of dsRNA-sensing pathways, achieved by combining E3, NSs and L*, is more effective than E3 alone in preventing saRNA-induced cell death and preserving cell viability.

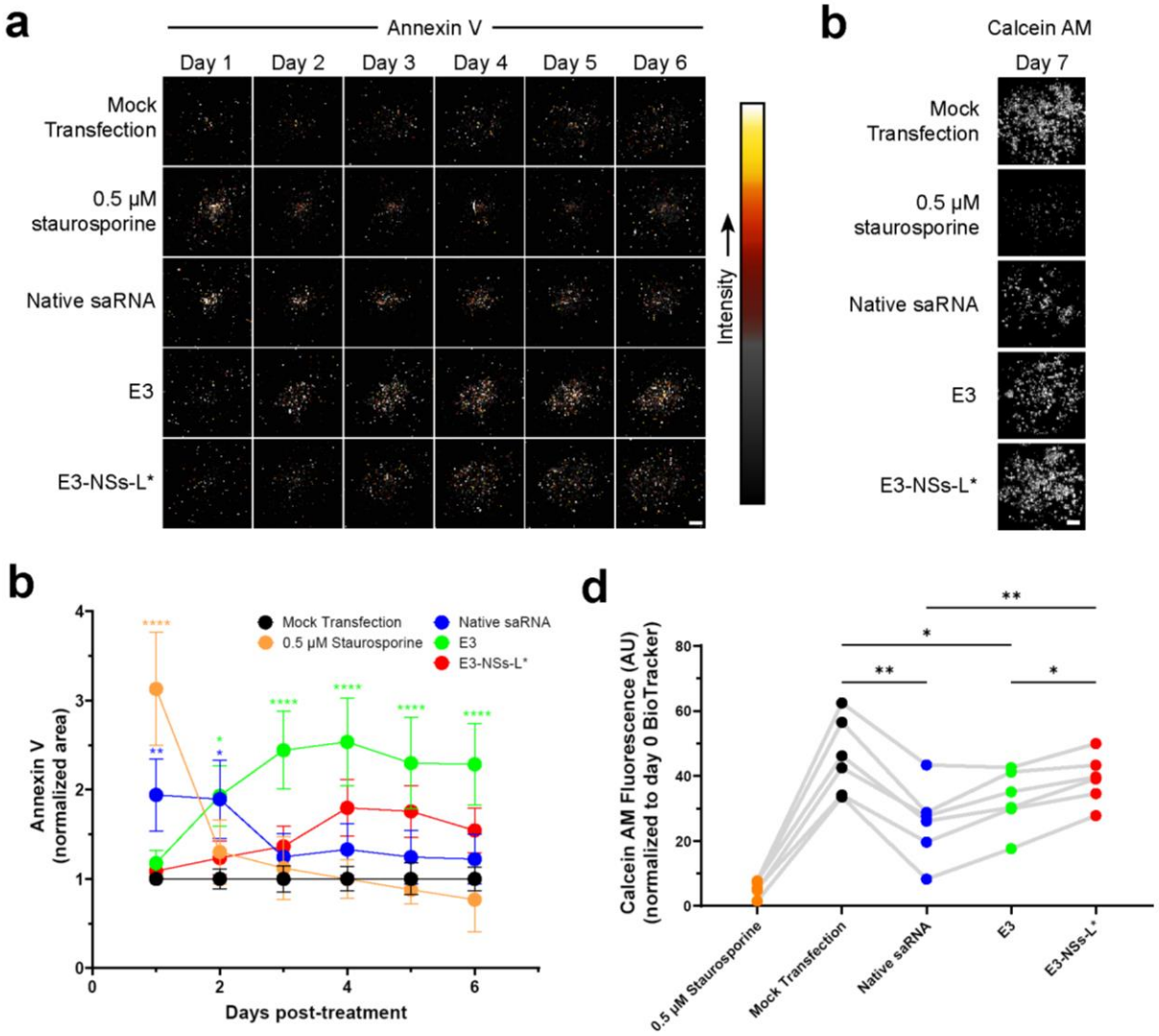

Fig. 2. saRNA induces increased phosphatidylserine staining and reduced viability, which is prevented by E3-NSs-L*

a, Representative cropped images of Annexin V-CF800 staining, indicating phosphatidylserine exposure or loss of membrane integrity, performed daily over 6 days using a microplate imager. Scale bar = 1.5 mm.

b, Representative cropped images of calcein AM staining, indicating viability, on day 7 post-treatment. Scale bar = 1.5 mm.

c, Annexin V staining, quantified as the area of positive pixels determined using Li thresholding (n = 6 biological replicates). Staurosporine, native saRNA, and the E3 construct significantly increased annexin V staining, while E3-NSs-L* did not. Data are normalized to the average of the mock transfection group. Statistical significance of treatment effects at each time point compared to mock transfection was determined using two-way RM ANOVA with Bonferroni's multiple comparisons test. Data are presented as mean ± SEM.
d, Calcein AM intensity measured on day 7 post-treatment (n = 6 biological replicates). Native saRNA, and E3 significantly reduced cell viability compared to mock transfection, while E3-NSs-L* did not. Cell viability in the E3-NSs-L* group was significantly higher than the E3 group. Connecting lines indicate responses from the same biological replicate. All groups differed significantly from staurosporine; these comparisons are omitted from the figure for clarity due to the large number of statistical comparisons. Data are normalized to cell number on day 0 as determined by BioTracker staining before transfection. Statistical significance was determined by one-way RM ANOVA with Greenhouse–Geisser correction and Tukey's multiple comparisons test comparing all groups.
saRNA constructs used are shown in Fig. 1a. For all statistical reporting, *P < 0.05, **P < 0.01, ***P < 0.001 and ****P < 0.0001.

E3 and E3-NSs-L prevent saRNA-induced eIF2α phosphorylation and differentially regulate eIF2α levels*

After characterizing how moderate and strong inhibition of dsRNA-sensing pathways affects saRNA-induced cytotoxicity, we next investigated molecular mechanisms of translational control to understand how this inhibition influences transgene expression. Eukaryotic initiation factor 2 alpha (eIF2α) is a central regulator of translation initiation; its phosphorylation serves as a cellular stress response to limit cellular cap-dependent protein synthesis, freeing ribosomes for cap-independent translation initiation instead.[48] Using in-cell western assays, we found that native saRNA transfection increased eIF2α phosphorylation, but both E3 and E3-NSs-L* effectively blocked this phosphorylation (Fig. 3a), consistent with previous reports of vaccinia virus E3's inhibitory effect on eIF2α phosphorylation.[22] Interestingly, E3-NSs-L* also increased total eIF2α levels, an effect not observed with the E3 construct (Fig. 3b).

E3-NSs-L counteracts saRNA-induced PKR upregulation*

Given that PKR phosphorylates eIF2α upon activation by dsRNA,[7] we next assessed its levels following saRNA transfection. Consistent with previous reports,[6] native saRNA transfection increased PKR levels (Fig. 3c). The E3 construct similarly increased PKR levels; however, co-expression of E3-NSs-L* mitigated this increase, suggesting that E3-NSs-L* effectively counteracts saRNA-induced PKR upregulation. This is in line with the known role of the Toscana virus NSs protein as a ubiquitin ligase that targets PKR for degradation.[39]

saRNA reduces eIF4E phosphorylation without altering total eIF4E levels

We next examined the impact of saRNA transfection on eIF4E, a key regulator of translation initiation.[49] All constructs reduced eIF4E phosphorylation levels (Fig 3d), while total eIF4E levels remained unchanged (Fig. 3e).

E3 reduces rRNA integrity, while E3-NSs-L protects against this reduction*

eIF2α- and eIF4E-mediated translational control do not account for the greater transgene expression observed with the E3 construct compared to the E3-NSs-L* construct. This is evidenced by the lack of significant differences in eIF2α and eIF4E phosphorylation status or levels between the two constructs (Figs. 3a-b, 3c-e), suggesting that additional mechanisms beyond eIF2α- and eIF4E-mediated control contribute to the enhanced transgene expression seen with the E3 construct.

When OAS binds dsRNA, it synthesizes 2′-5′-oligoadenylate, which activates RNase L to cleave single-stranded RNA, leading to cellular mRNA degradation[50] and inhibition of mRNA nuclear export,[51] thereby massively reducing host protein synthesis.[52] Many RNA viruses, including dengue and Zika, evade RNase L by localizing their transcripts within viral replication organelles, protecting them from degradation while allowing continued protein production.[51,53] Similarly, the VEEV-derived saRNA used in this study replicates within these organelles,[54] likely protecting its transcripts from RNase L activity. Consequently, RNase L activation by the E3 construct may selectively deplete cytoplasmic host mRNA while sparing saRNA. This depletion reduces competition for ribosomes, thereby enhancing the translation of saRNA transcripts. In contrast, the E3-NSs-L* construct encodes Theiler's virus L*, an RNase L inhibitor,[40] thereby preventing host mRNA degradation and forcing saRNA transcripts to compete directly with cellular mRNA for ribosomal access.

To determine whether RNase L activation contributes to the greater transgene expression observed with the E3 construct compared to E3-NSs-L*, we assessed RNase L activity by measuring ribosomal RNA (rRNA) cleavage, an indicator of RNase L activity.[55] RNA extracted from FLS transfected with the E3 and E3-NSs-L* constructs was evaluated with the RNA integrity number (RIN) algorithm, an automated Bayesian learning method for assessing rRNA integrity.[56] Cells transfected with E3 exhibited significantly lower rRNA integrity than those transfected with E3-NSs-L* (Fig. 3f). As prior studies have shown that RNase L activation primarily depletes host mRNA levels before extensive rRNA degradation,[50,52,57] our findings support the hypothesis that RNase L activation and subsequent reductions in cellular mRNA occur with the E3 construct but not with E3-NSs-L*.

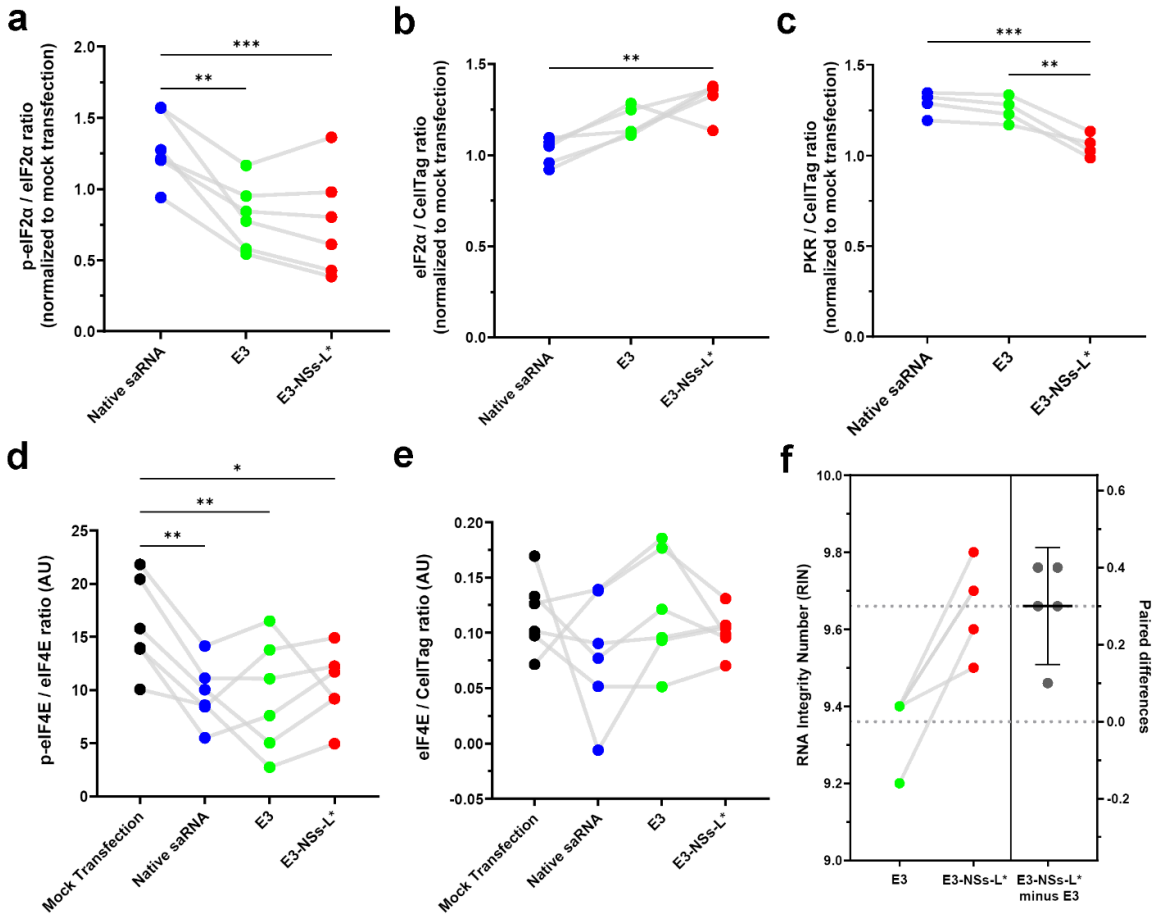

Fig. 3. Translational control alterations induced by saRNA are modulated by dsRNA-sensing pathway inhibitors with differing effects on RNA integrity

a, Phosphorylated eIF2α levels examined day 2 post-transfection by in-cell western assay (n = 6 biological replicates). Both E3 and E3-NSs-L* constructs significantly reduced eIF2α phosphorylation. Data are presented as fold-change relative to mock transfected cells. Statistical significance was determined by one-way RM ANOVA with Tukey's multiple comparisons test.
b, eIF2α levels examined day 2 post-transfection by in-cell western assay (n = 5 biological replicates). E3-NSs-L* significantly increased total eIF2α levels compared to native saRNA transfection. Data are presented as fold-change relative to mock transfected cells. Statistical significance was determined by one-way RM ANOVA with Tukey's multiple comparisons test.
c, PKR levels examined day 2 post-transfection by in-cell western assay (n = 4 biological replicates). E3-NSs-L* significantly reduced PKR levels compared to both native saRNA and E3 transfection. Data are presented as fold-change relative to mock transfected cells. Statistical significance was determined by one-way RM ANOVA with Tukey's multiple comparisons test.
d, Phosphorylated eIF4E levels examined day 2 post-transfection by in-cell western assay (n = 6 biological replicates). All saRNA constructs tested significantly reduced eIF4E phosphorylation levels compared to mock transfection. Statistical significance was determined by one-way RM ANOVA with Tukey's multiple comparisons test.
e, eIF4E levels examined day 2 post-transfection by in-cell western assay (n = 6 biological replicates). One-way RM ANOVA revealed no significant differences between groups ($F(3,15) = 1.207$, $P = 0.3410$).
f, rRNA integrity of FLS transfected with E3-NSs-L* is significantly higher than that of E3-transfected FLS (n = 5 biological replicates). rRNA integrity was assessed using the RNA Integrity Number (RIN) algorithm, which ranges from 1 to 10, with 10 indicating fully intact rRNA. Total RNA was extracted from FLS 1 day post-transfection. Data are shown as a Gardner-Altman comparison plot, with the right panel illustrating the mean effect size ± 95% CI. Statistical significance was assessed using a paired t-test ($P = 0.0054$).
saRNA constructs used are shown in Fig. 1a. Connecting lines indicate responses from the same biological replicate. Statistical significance is indicated as follows: *$P < 0.05$, **$P < 0.01$, ***$P < 0.001$. The mock transfection control data presented in panels (a), (b), (d) and (f) are also used in Fig. 6.

Design of saRNA constructs for inhibiting multiple inflammatory signaling pathways

Having addressed key saRNA-induced toxicities—including cell death, translation shutdown, and mRNA degradation—with the E3-NSs-L* construct, we next sought to design new saRNA constructs aimed at mitigating cytokine production. In these new constructs, E3-NSs-L*-EGFP was expressed via a single IRES using non-identical 2A peptides (Fig. 4a). On a second IRES, varying amounts of cellular inhibitors of inflammatory signaling were expressed. The control construct, called 'moxBFP', lacks cellular inhibitors of inflammatory signaling and instead expresses a blue fluorescent protein.

Given that activation of nuclear factor-κB (NF-κB) is a hallmark of viral infection and a master regulator of cytokine and chemokine induction,[58,59] we prioritized its inhibition using super repressor inhibitor of κBα (srIκBα). This dominant active form of IκBα cannot be phosphorylated and thus resists ubiquitination and degradation, forming a stable cytoplasmic pool of IκBα that prevents NF-κB nuclear translocation and downstream signaling.[60,61] We generated one construct expressing srIκBα alone (named 'srIκBα') and another expressing srIκBα in combination with Smad7 and suppressor of cytokine signaling 1 (SOCS1) using non-identical 2A peptides (named 'srIκBα-Smad7-SOCS1'). Smad7 negatively regulates both transforming growth factor-β (TGF-β) and NF-κB signaling pathways,[62] while SOCS1 inhibits type I, II, and III interferon (IFN) pathways as well as NF-κB signaling.[63–65]

Inhibiting dsRNA-sensing pathways and inflammatory signaling suppresses saRNA-induced cytokine secretion

Using a bead-based immunoassay on FLS culture supernatants, we observed that native saRNA transfection induced cytokine responses associated with viral infection (Figs. 4b, S4a-m). Cytokine secretion was still apparent when dsRNA-sensing pathways were inhibited, although a reduction in tumor necrosis factor (TNF)-α, IFN-α, and IFN-β levels were observed with E3 expression. Similarly, C-X-C motif chemokine ligand 10 (CXCL10) levels were reduced with E3-NSs-L* expression. On the other hand, srIκBα co-expression broadly suppressed cytokine secretion, reducing all measured cytokines to levels comparable to mock-transfected FLS. The srIκBα-Smad7-SOCS1 construct did not further reduce cytokine levels beyond the suppression achieved by srIκBα alone.

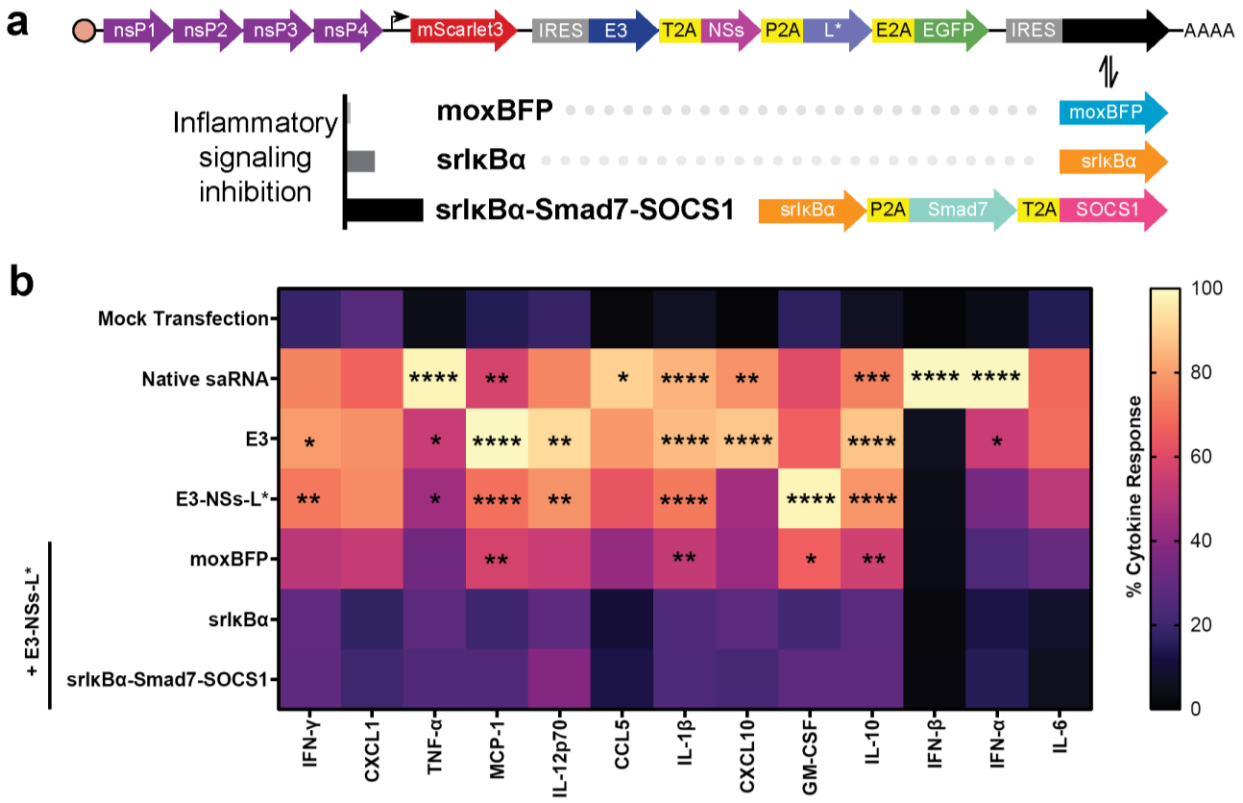

Fig. 4. Inhibiting inflammatory signaling reduces saRNA-induced anti-viral cytokine secretion

a, Schematic of the moxBFP, srIκBα, and srIκBα-Smad7-SOCS1 saRNA constructs designed for inhibition of inflammatory signaling. These constructs include dsRNA-sensing pathway inhibitors (vaccinia virus E3, Toscana virus NSs, and Theiler's virus L*). The moxBFP construct, serving as a control, lacks inflammatory signaling inhibitors. The srIκBα construct co-expresses srIκBα, which blocks the NF-κB inflammatory signaling pathway and represents moderate inflammatory signaling inhibition. The srIκBα-Smad7-SOCS1 construct co-expresses srIκBα, Smad7 and SOCS1 to additionally inhibit TGF-β and IFN pathways, representing strong inflammatory signaling inhibition. The angled arrow denotes the subgenomic promotor.
b, FLS were transfected with saRNA constructs, and anti-viral cytokines were quantified by bead-based immunoassay on day 2 post-transfection (n = 6 biological replicates). dsRNA-sensing pathway inhibition and inflammatory signaling inhibition significantly reduced cytokine secretion induced by saRNA. Cytokine levels were scaled within each biological replicate, with the highest value set to 100%, and the mean

value displayed in the heatmap. Detailed graphs of individual cytokines are shown in Supplementary Fig. S4. For statistical analysis, cytokine levels were normalized to pre-transfection cell number (measured using BioTracker). Statistical significance for each cytokine was assessed using one-way RM ANOVA followed by Bonferroni's multiple comparisons test against the mock transfection control. A Bonferroni correction was applied to P values to account for multiple independent hypothesis testing. *$P < 0.05$, **$P < 0.01$, ***$P < 0.001$ and ****$P < 0.0001$.

Acronyms: nsP, Venezuelan equine encephalitis virus non-structural protein; IRES, encephalomyocarditis virus internal ribosome entry site; moxBFP, monomeric oxidizing environment-optimized blue fluorescent protein; E3, Vaccinia virus E3 protein; NSs, Toscana virus non-structural NSs protein; L*, Theiler's murine encephalomyelitis virus L* protein; T2A, Thosea asigna virus 2A peptide; P2A, porcine teschovirus-1 2A peptide, E2A, equine rhinitis A virus 2A peptide, srIκBα, super-repressor inhibitor of κBα; smad7, mothers against decapentaplegic homolog 7; SOCS1, suppressor of cytokine signaling 1; IFN-γ, interferon-γ; CXCL1, C-X-C motif chemokine ligand 1; TNF-α, tumor necrosis factor-α; MCP-1, monocyte chemoattractant protein-1; IL-12p70, interleukin-12; CCL5, chemokine ligand 5; IL-1β, interleukin-1β; CXCL10, C-X-C motif chemokine ligand 10; GM-CSF, granulocyte-macrophage colony-stimulating factor; IL-10, interleukin-10; IFN-β, interferon-β; IFN-α, interferon-α; IL-6, interleukin-6.

srIκBα* reduces cell number, whereas *srIκBα-Smad7-SOCS1 preserves cell number and enhances transgene expression

We then examined the impact of inhibiting inflammatory signaling on cell number and transgene expression (Figs. 5a, 5b). Interestingly, the srIκBα construct caused both immediate and sustained reductions in cell number, as quantified by BioTracker signal, whereas the srIκBα-Smad7-SOCS1 construct maintained cell number comparable to mock transfection throughout the experiment (Fig. 5c). AUC analysis of the BioTracker data confirmed that srIκBα-Smad7-SOCS1 significantly mitigated the srIκBα-induced reduction in integrated BioTracker signal (Fig. S5a). Additional experiments using CellTag and calcein AM staining corroborated these findings, showing that srIκBα negatively impacted both cell number (Fig. S5b) and viability (Fig. S5c), effects that were prevented by co-expression of Smad7 and SOCS1.

All three constructs produced low levels of EGFP expression (Fig. 5d), which was expected given EGFP's position as the fourth protein in a quad-cistronic 2A element (Fig. 4a). Previous studies have demonstrated that protein expression decreases significantly for downstream genes in such configurations.[41] Notably, while the moxBFP and srIκBα constructs generated intermediate mScarlet3 levels, the srIκBα-Smad7-SOCS1 construct produced 2- to 5-fold higher mScarlet3 fluorescence compared to the others (Fig. 5e).

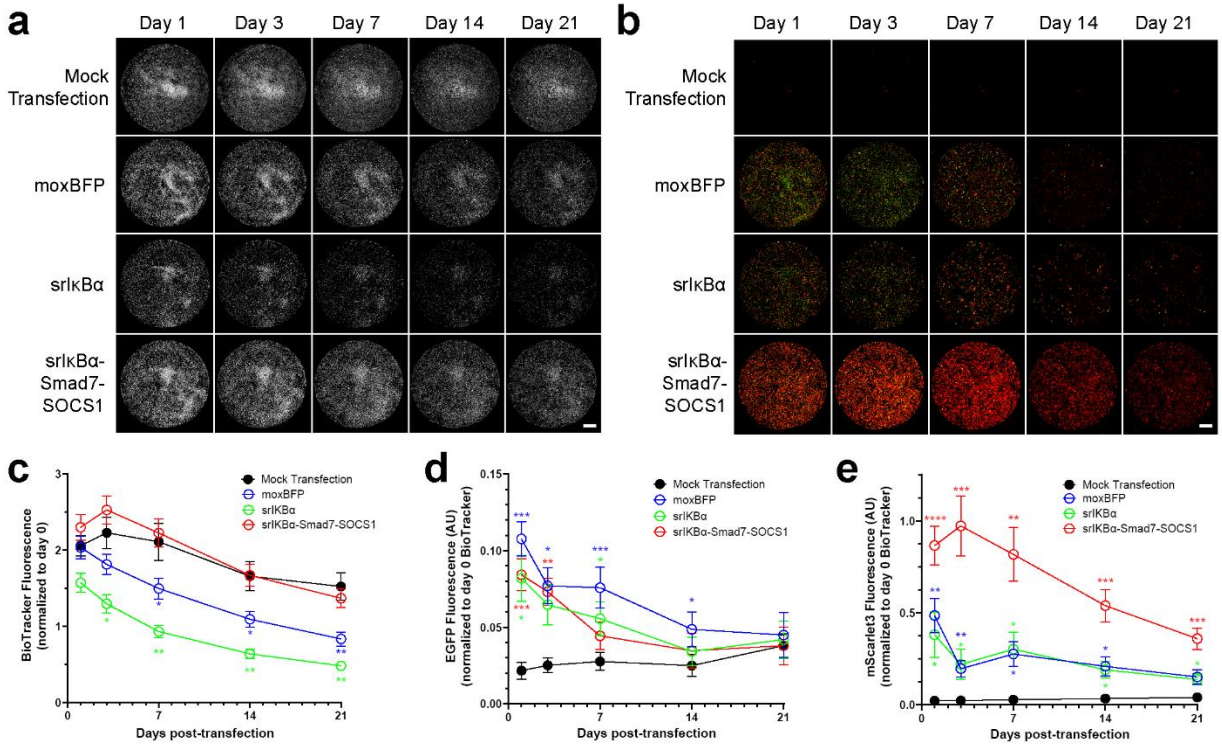

Fig. 5. Differential effects of srIκBα and srIκBα-Smad7-SOCS1 on cell number and transgene expression.

a, Representative images of BioTracker staining over 3 weeks in FLS transfected with different saRNA constructs. Scale bar = 5 mm.
b, Representative images of EGFP (green) and mScarlet3 (red) expression over 3 weeks in FLS transfected with different saRNA constructs. Scale bar = 5 mm.
c, Quantification of BioTracker fluorescence intensity over time (n = 11 biological replicates). srIκBα induces reduction in cell number, which is prevented by srIκBα-Smad7-SOCS1. Statistical significance of treatment effects at each time point compared to mock transfection was determined by two-way RM ANOVA with Greenhouse–Geisser correction and Dunnett's multiple comparisons test.
d, Quantification of EGFP fluorescence intensity over time (n = 11 biological replicates). All constructs showed low levels of EGFP expression. Statistical significance of treatment effects at each time point compared to mock transfection was determined by two-way RM ANOVA with Greenhouse–Geisser correction and Dunnett's multiple comparisons test.
e, Quantification of mScarlet3 fluorescence intensity over time (n = 11 biological replicates). The srIκBα-Smad7-SOCS1 produced 2-5 times more mScarlet3 fluorescence than either moxBFP or srIκBα constructs. Statistical significance of treatment effects at each time point compared to mock transfection was determined by two-way RM ANOVA with Greenhouse–Geisser correction and Dunnett's multiple comparisons test.
saRNA constructs used are shown in Fig. 4a. For all statistical reporting, *P < 0.05, **P < 0.01, ***P < 0.001 and ****P < 0.0001. Data were normalized to cell number (BioTracker intensity) on day 0, prior to transfection. The mock transfection control data used in this figure is also presented in Fig. 1. Data are presented as mean ± SEM.

Smad7 and SOCS1 co-expression prevents srIκBα-induced alterations in translational control

We next explored how srIκBα and srIκBα-Smad7-SOCS1 modulate translational regulation. Interestingly, srIκBα expression led to reductions in eIF2α phosphorylation, a change that was prevented by co-expression of Smad7 and SOCS1 (Fig. 6a). While neither construct affected total eIF2α levels or eIF4E phosphorylation compared to the moxBFP construct (Figs. 6b, 6c), srIκBα caused a significant reduction in total eIF4E levels (Fig. 6d). Given the critical role of eIF4E in cap-dependent translation, its depletion likely contributes to the poor transgene expression observed with srIκBα (Fig. 5e). These effects, combined with srIκBα-induced declines in cell number and viability (Figs. 5c, S5a-c), highlight the dual impact of srIκBα on translational machinery and cellular health. Importantly, Smad7 and SOCS1 co-expression preserved eIF4E levels, counteracting the disruption of cap-dependent translation caused by srIκBα.

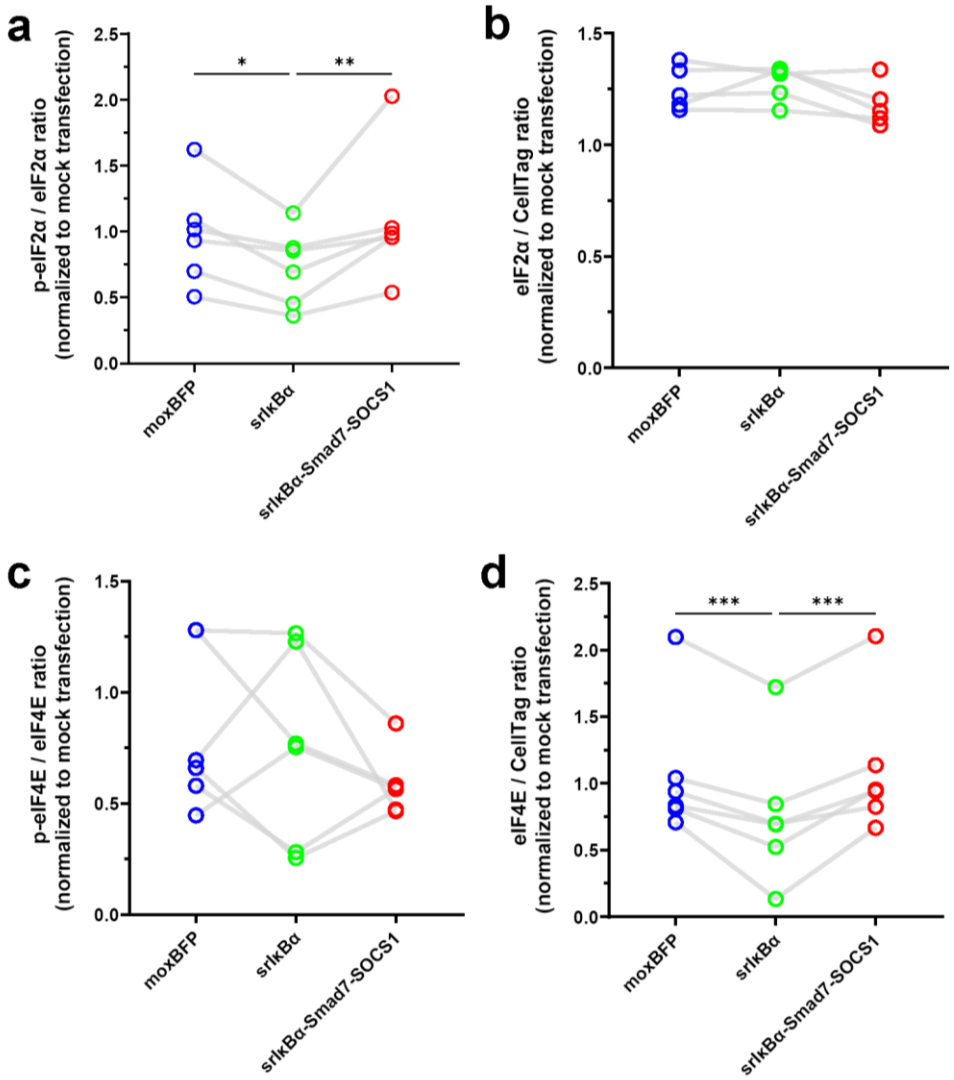

Fig. 6. ***srIκBα reduces eIF2α phosphorylation and total eIF4E levels, effects reversed by co-expression of Smad7 and SOCS1***

In-cell western assays were performed 2 days post-transfection. Data are presented as fold change relative to mock-transfected cells.

a, Phosphorylation of eIF2α is significantly reduced by srIκBα, and this reduction is reversed by co-expression of Smad7 and SOCS1 (n = 6 biological replicates). Statistical significance was determined by one-way RM ANOVA and Holm-Šídák's multiple comparisons test to compare all groups.
b, Total eIF2α levels are not significantly affected by srIκBα or srIκBα-Smad7-SOCS1 (n = 6 biological replicates). One-way RM ANOVA revealed no significant differences among groups. F(2,8)=3.683, P=0.0735.
c, Phosphorylation of eIF4E is not significantly affected by srIκBα or srIκBα-Smad7-SOCS1 (n = 6 biological replicates). One way RM ANOVA revealed no significant difference among groups. F(2,10)=1.336, P=0.3059.
d, Total eIF4E levels are significantly reduced by srIκBα, an effect reversed by co-expression of Smad7 and SOCS1 (n = 6 biological replicates). Statistical significance was determined by one-way RM ANOVA and Holm-Šídák's multiple comparisons test to compare all groups.
saRNA constructs are described in Fig. 4a. Connecting lines indicate responses from the same biological replicate. For all statistical reporting, *P < 0.05, **P < 0.01 and ***P < 0.001. Mock transfection data used for normalization are the same as in Fig. 3.

Prolonged moxBFP transfection does not activate FLS, while srIκBα reduces basal activation

Fibroblast activation protein-α (FAP-α) is a serine protease expressed on the surface of FLS that contributes to extracellular matrix degradation and tissue remodeling.[66,67] Its expression is minimal in normal adult FLS but increases significantly following inflammatory activation, such as in rheumatoid and osteoarthritis.[68,69] Since viral infections can induce fibroblast activation,[70,71] we hypothesized that prolonged saRNA transfection might similarly trigger FLS activation. To test this, we measured FAP-α levels using an in-cell western assay after 11 days of transfection. FLS transfected with moxBFP showed FAP-α levels comparable to those of mock-transfected cells, whereas srIκBα and srIκBα-Smad7-SOCS1 constructs resulted in significantly lower FAP-α levels compared to mock transfection (Figs. 7a, 7b). These findings indicate that long-term saRNA transfection does not induce FLS activation, as measured by FAP-α levels, potentially alleviating concerns that saRNA might drive pathological fibroblast responses.

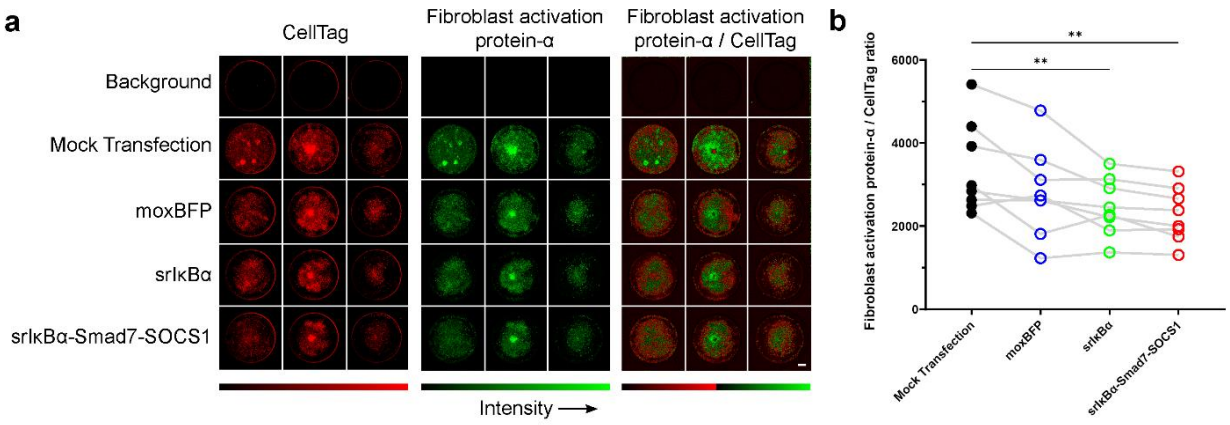

Fig. 7. Prolonged transfection with *srIκBα or srIκBα-Smad7-SOCS1 significantly reduces basal fibroblast activation factor-α (FAP-α) levels*

a, Representative in-cell western images showing FAP-α expression. Columns show different biological replicates, and rows show different treatments. The montage on the right shows FAP-α signal normalized to CellTag signal (FAP-α/CellTag).

b, In-cell western assay of FAP-α expression (n = 8 biological replicates). Both srIκBα and srIκBα-Smad7-SOCS1 significantly reduce FAP-α levels compared to mock transfection, while moxBFP does not differ significantly from mock. Statistical significance was determined by one-way RM ANOVA with Greenhouse–Geisser correction and Dunnett's multiple comparisons test to compare groups to mock transfection. Connecting lines indicate responses from the same biological replicate. **P<0.01.

External control of transgene expression using a small-molecule antiviral

The srIκBα-Smad7-SOCS1 construct, which includes E3-NSs-L*, provides broad suppression of dsRNA sensing and inflammatory signaling pathways. This construct mitigates saRNA-induced cytokine release (Figs. 4b, S4a-m) and counters saRNA- and srIκBα-induced reductions in cell viability (Figs. 5c, S5a–c), enabling sustained cap-dependent transgene expression (Fig. 5e) without inducing fibroblast activation (Fig. 7b) or causing srIκBα-associated reductions in eIF4E levels (Fig. 6d). Together, these attributes position the srIκBα-Smad7-SOCS1 construct as a promising candidate for transient gene therapy applications.

To further enhance the therapeutic potential of this construct, we investigated the possibility of using a small-molecule drug to halt transgene expression. Achieving temporal control of transgene expression would enhance safety and flexibility in therapeutic contexts. The saRNA constructs in this study rely on the VEEV RdRp for self-amplification. VEEV is a mosquito-borne alphavirus capable of causing flu-like illness in humans, with the potential to progress to fatal encephalitis.[72] Due to its pathogenicity, significant efforts have focused on developing small-molecule inhibitors of VEEV. One such compound is ML336, a potent inhibitor of the VEEV RdRp.[73]

To test whether ML336 could inhibit transgene expression of the srIκBα-Smad7-SOCS1 construct, ML336 or vehicle was added to the culture medium one day post-transfection. EGFP and mScarlet3 fluorescence were monitored over 13 days (Fig. 8a), followed by calcein AM staining to assess cell viability (Fig. 8b). ML336 treatment significantly reduced EGFP and mScarlet3 expression over time (Figs. 8c, 8d), demonstrating its efficacy in controlling saRNA transgene expression. While vehicle-treated cultures exhibited lower viability compared to mock-transfected cells—possibly due to reduced proliferation over the experiment's duration—prolonged ML336 treatment did not reduce viability relative to mock-transfected controls (Fig. 8e).

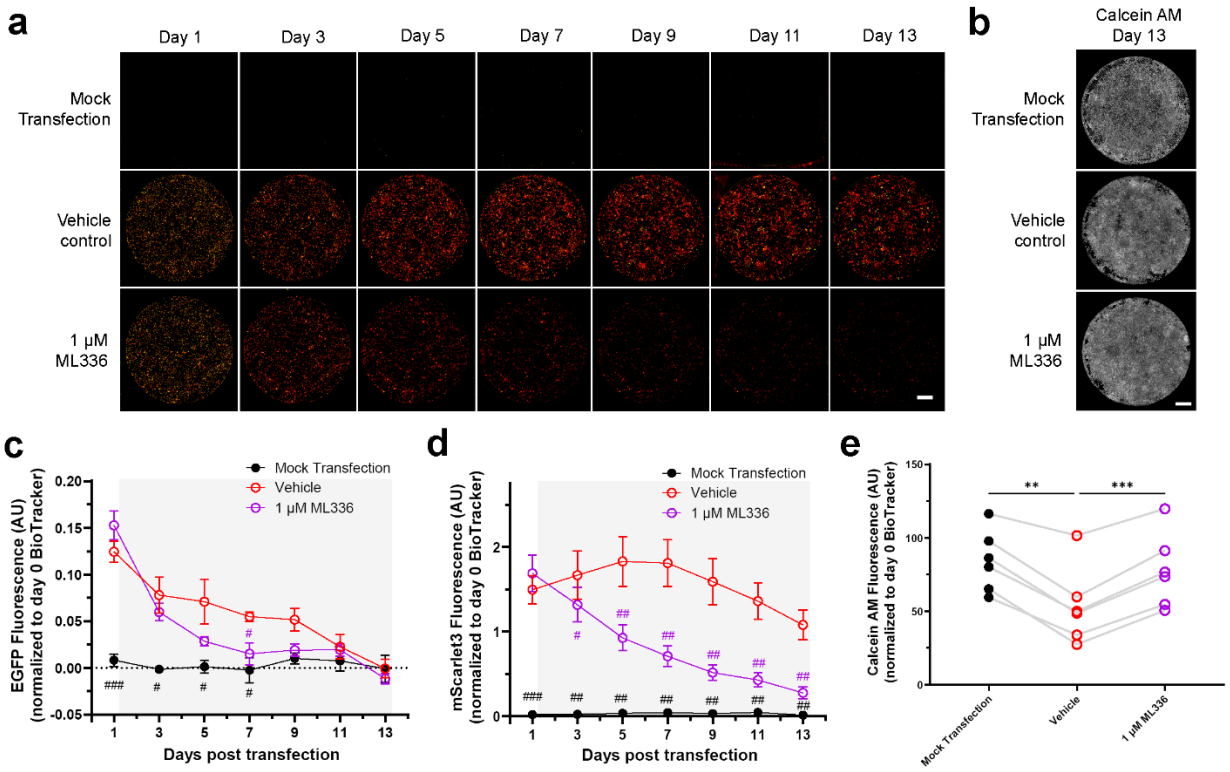

Fig. 8. ML336 enables external control of transgene expression from the srIκBα-Smad7-SOCS1 construct

a, Representative images of EGFP (green) and mScarlet3 (red) expression over 13 days in FLS transfected with srIκBα-smad7-SOCS1. Cultures were treated with vehicle or 1 μM ML336, starting 1 day post-transfection. Scale bar = 5 mm.
b, Representative images of calcein AM staining on day 13 post-transfection. Scale bar = 5 mm.
c, Quantification of EGFP fluorescence intensity in srIκBα-Smad7-SOCS1-transfected FLS (n = 6 biological replicates). Cultures were treated with vehicle or 1 μM ML336 (treatment period indicated by shading). EGFP fluorescence was significantly lower in ML336-treated cultures compared to vehicle-treated cultures on day 7. Statistical significance relative to vehicle-treated cells was determined by two-way RM ANOVA with Greenhouse–Geisser correction and Dunnett's multiple comparisons test. #P<0.05, ###P<0.01.
d, Quantification of mScarlet3 fluorescence intensity in srIκBα-Smad7-SOCS1-transfected FLS (n = 6 biological replicates). Cultures were treated with vehicle or 1 μM ML336 (treatment period indicated by shading). mScarlet3 fluorescence was significantly lower in ML336-treated cultures compared to vehicle-treated cultures beginning on day 3. Statistical significance relative to vehicle-treated cells was determined by two-way RM ANOVA with Greenhouse–Geisser correction and Dunnett's multiple comparisons test. #P<0.05, ##P<0.01, ###P<0.001.
e, Quantification of calcein AM staining on day 13 post-transfection, following 12 days of vehicle or ML336 treatment (n = 6 biological replicates). Cultures treated with ML336 showed no significant difference in calcein AM signal compared to mock transfection, while vehicle-treated cultures exhibited significantly lower calcein AM signals compared to both mock-transfected and ML336-treated cultures. Connecting lines indicate responses from the same biological replicate. Statistical significance was determined by one-way RM ANOVA with Greenhouse–Geisser correction and Tukey's multiple

comparisons test. **P<0.01, ***P<0.001.
Data were normalized to BioTracker intensity on day 0 and are presented as mean ± SEM.

DISCUSSION

saRNA-induced translation shutdown is thought to be mediated by phosphorylation of eIF2α.[22,74,75] During saRNA replication, dsRNA replicative intermediates activate PKR, leading to eIF2α phosphorylation and translation inhibition.[7,22] Our study is consistent with this mechanism and additionally demonstrates that saRNA induces a reduction in eIF4E phosphorylation, a phenomenon previously observed with alphavirus replicons, although the underlying mechanism remains unclear.[76,77] Similar to eIF2α phosphorylation,[78] a reduction in eIF4E phosphorylation decreases global cap-dependent translation initiation,[79] promoting cap-independent translation.[80] These combined effects—phosphorylation of eIF2α and reduced phosphorylation of eIF4E—may explain why IRES-driven, cap-independent transgenes often achieve higher expression compared to those relying on cap-dependent expression when using native saRNA.[26,81]

To counteract saRNA-induced translation shutdown, we designed saRNA constructs that express inhibitors targeting dsRNA-sensing pathways using IRES-mediated translation. During translation shutdown, global mRNA translation decreases, freeing ribosomes that would otherwise be used for translating capped mRNAs, thereby enhancing cap-independent translation.[82] By leveraging this mechanism, IRES-mediated expression of dsRNA-sensing pathway inhibitors ensures their levels increase as translation shutdown intensifies. This approach effectively inhibits dsRNA sensing and alleviates translation shutdown. In contrast, encoding these inhibitors via cap-dependent translation is expected to be less effective, as translation shutdown would lead to reduced inhibitor expression.

In this study, we used vaccinia virus E3 to prevent saRNA-induced translation shutdown, a role that E3 has previously been used to fulfill.[22,23] E3 achieves this by sequestering dsRNA intermediates from sensors like PKR[83] and by directly inhibiting PKR activation.[84] These dual actions prevent eIF2α phosphorylation, alleviating translation inhibition and enhancing transgene expression.[22,23] However, our findings suggest that this mechanism is incomplete. While E3 prevents saRNA-induced eIF2α phosphorylation, its ability to enhance transgene expression also depends on RNase L activity. By alleviating translation inhibition, E3 facilitates unrestrained RdRp production, driving robust saRNA replication and dsRNA synthesis. This dsRNA activates RNase L, which degrades mRNA[50] and inhibits nuclear mRNA export.[51] The resulting depletion of cytoplasmic mRNA[52] reduces competition for ribosomes, enabling enhanced translation of saRNA transcripts. These transcripts are shielded from RNase L degradation due to their localization within plasma membrane-associated micro-compartments called spherules.[3] Consistent with this model, inhibiting RNase L with L* in the E3-NSs-L* construct reduced transgene expression, likely due to restored ribosomal competition from intact host mRNA.

While preventing eIF2α phosphorylation and activating RNase L drive high levels of saRNA transgene expression, this combination also causes significant cytotoxicity with the E3 construct. This dual-edged effect potentially makes the E3 construct suited for immunotherapy applications, such as vaccines and cancer therapy, where robust transgene expression and immunogenic cell death can promote strong immune responses.[85,86] In contrast, non-immunotherapy applications require strategies that prioritize cell viability and minimize tissue damage over maximizing transgene expression.

Alphavirus vectors, including the VEEV replicon used in this study, are known to induce cytotoxicity in mammalian cells.[6,10,12–16] This cytotoxicity arises from dsRNA intermediates, which activate sensors such as PKR, RIG-I, MDA-5, and OAS,[5,7,22,87] despite partial shielding within spherules.[3,74] Studies in HeLa cells using microinjected dsRNA show that PKR is essential for cytosolic dsRNA-induced apoptosis, while RIG-I and MDA-5 are dispensable.[88] Numerous studies further underscore the central role of PKR in

mediating apoptosis in response to dsRNA,[89–91] and have shown that PKR can mediate dsRNA-induced apoptosis even in the absence of eIF2α phosphorylation.[92] OAS also contributes to dsRNA-induced apoptosis by producing 2'-5'-oligoadenylates upon binding dsRNA, which activate RNase L, leading to cleavage of single-stranded RNA.[52] This disrupts cellular translation as cleavage of actively translated mRNA causes ribosome stalling. Ribosomes encountering truncated 3' ends of mRNAs are unable to dissociate, resulting in collisions,[93,94] triggering the ribotoxic stress response[95] which can lead to apoptosis.[93,96] These findings from the literature identify PKR and OAS/RNase L as key contributors to saRNA-associated cytotoxicity and highlight them as valuable targets for mitigation.

While E3 relieves saRNA-induced eIF2α phosphorylation,[22,23] the E3 construct also compromised RNA integrity, suggesting activation of the OAS/RNase L pathway. Furthermore, PKR, an IFN-inducible gene,[97] was upregulated by the E3 construct, potentially allowing partial evasion of E3-mediated inhibition. Thus, vaccinia virus E3 alone did not fully address the cytotoxic actions of dsRNA replicative intermediates produced during saRNA replication. To further suppress PKR and OAS/RNase L pathways, we used Toscana virus NSs[39] and Theiler's virus L*,[40] respectively. While this strategy resulted in lower transgene expression—likely due to the protective actions of RNase L inhibition on cellular mRNA integrity—it effectively mitigated the intrinsic mechanisms of saRNA cytotoxicity. However, the inclusion of multiple viral proteins introduces additional challenges. *In vivo*, saRNA constructs must contend not only with intrinsic cytotoxic mechanisms but also with adaptive immune responses leading to extrinsic cytotoxicity. The co-expression of several viral proteins, along with the VEEV RdRp, significantly increases the likelihood of viral peptides being presented on major histocompatibility complex class I molecules to cytotoxic T lymphocytes. This is expected to activate adaptive immune responses, which could culminate in the elimination of saRNA-transfected cells. Addressing both intrinsic and immune cell-mediated cytotoxicity will be critical to achieving the long-term viability of saRNA-transfected cells and unlocking the platform's full therapeutic potential.

While we found that inhibiting dsRNA-sensing pathways was an effective means to reduce saRNA-induced cytotoxicity, it was not effective at preventing saRNA-induced cytokine responses. This agrees with prior reports showing that dsRNA activates NF-κB even in the absence of PKR and RNase L,[98] suggesting additional mechanisms contribute to NF-κB activation. One such mechanism may involve eIF4E, a key regulator of translation initiation, whose activity is governed by its phosphorylation status and serves as a rate-limiting step in cap-dependent protein synthesis.[49] In this study, we found that saRNA transfection induces a reduction in eIF4E phosphorylation. Reduced eIF4E phosphorylation has been shown to decrease the levels of the short-lived IκBα protein,[99] an inhibitor of NF-κB that sequesters it in the cytoplasm and prevents nuclear translocation. Decreased IκBα levels thus allow NF-κB to translocate to the nucleus, initiating cytokine expression and inflammatory responses. To address this, we expressed srIκBα using cap-independent translation to produce a stable cytoplasmic pool of IκBα, thereby preventing NF-κB activity. While this strategy effectively reduced saRNA-induced cytokine responses, it also resulted in a reduction in cell viability.

The NF-κB pathway is a key regulator of inflammatory cytokine production, making it an important target for suppressing cytokine responses.[100] However, NF-κB also has pro-survival functions as it promotes the transcription of anti-apoptotic genes—though its exact effects depend on tissue type and biological context.[101] In FLS, overexpression of srIκBα reduces inflammatory cytokine production but increases sensitivity to TNF-α-induced apoptosis,[102,103] consistent with our findings that saRNA encoding srIκBα lowered both anti-viral cytokine responses and cell viability. This phenomenon is not unique to FLS; inhibition of NF-κB signaling with srIκBα has also been shown to render liver hepatocytes more susceptible to pro-apoptotic stimuli.[104] This raises a key safety consideration, as saRNA delivery systems such as lipid nanoparticles tend to accumulate in the liver.[105] Therefore, when designing saRNA constructs for sustained, non-immunostimulatory transgene expression in contexts where apoptosis is

undesirable, the use of srIκBα to suppress cytokine responses may require co-expression of anti-apoptotic proteins to offset the loss of NF-κB-mediated survival signaling.

In this study, we show that co-expressing Smad7 and SOCS1 effectively counteracted srIκBα-induced cell death in FLS. While we did not assess the individual contributions of each protein, both are known to have anti-apoptotic properties in certain contexts. Smad7 can inhibit TGF-β-induced apoptosis,[106,107] while SOCS1 can suppress apoptosis triggered by IFN-α, IFN-β,[108] IFN-γ,[109] and TNF-α.[110–112] These anti-apoptotic effects likely enable Smad7 and SOCS1 to mitigate srIκBα-induced reductions in FLS cell viability.

We also found that co-expression of Smad7 and SOCS1 significantly enhanced cap-dependent transgene expression. Although we did not distinguish the contributions of each protein to this effect, it is likely mediated by SOCS1. Previous studies have shown that ruxolitinib, a small-molecule inhibitor of Janus kinase (JAK) 1 and JAK2,[113] increases saRNA transgene expression when added to saRNA polyplexes.[18] SOCS1 is an endogenous inhibitor of JAK1 and JAK2,[114] therefore, SOCS1 offers a genetically encoded alternative to the small-molecule approach of ruxolitinib for enhancing saRNA expression.

Furthermore, this study presents a straightforward method for controlling saRNA activity. ML336, a VEEV RdRp inhibitor, blocks the synthesis of positive-sense genomic, negative-sense template, and subgenomic RNAs of VEEV without affecting host cellular RNA transcription.[115] It has an *in vitro* effective concentration 50 (EC_{50}) of 0.02-0.04 μM, and a 50 mg/kg dose offers 100% protection in a lethal VEEV mouse infection model, with no observed toxicity.[116] Thus, ML336 and other RdRp inhibitors could provide a practical means to deactivate saRNA—either to terminate transgene expression once therapeutic objectives are met or as a safety measure to reduce the risks associated with prolonged innate immune suppression and other potential side effects, including adaptive immune responses to the VEEV replicon or viral innate immune inhibitory proteins.

Preclinical and clinical data show that saRNA vaccines often trigger an intense innate immune response that can hinder antigen expression.[8,18,22] Additionally, saRNA vaccines can induce significant inflammation,[117,118] which is increasingly recognized as problematic, as common adverse events include pain, headache, tenderness, arthralgia, fever, and chills.[119,120] The approaches described in this study, which reduces the inherent immunostimulatory effects of saRNA replication, could potentially be applied to future saRNA vaccine designs to improve antigen expression and reduce reactogenicity.

The approach in this study also underscores the versatility of the saRNA platform, which can efficiently integrate multiple transgenes and genetic elements. Our largest construct included the VEEV RdRP, two IRES sequences, five 2A peptides, and eight transgenes within a 16.5-kilobase saRNA. This ability to encode numerous transgenes without apparent size constraints is a notable yet underutilized strength of the saRNA platform.

Leveraging this capacity for multiple transgenes, we encoded diverse inhibitors of dsRNA-sensing and inflammatory signaling pathways directly within saRNA achieving durable and controllable transgene expression with minimal cytotoxicity and immunostimulation. This approach eliminates the need for exogenous immune suppressants, a common requirement in other studies utilizing saRNA for non-immunotherapy applications. For instance, therapeutic antibody production, cellular reprogramming, and retinal cell transfection with saRNA have relied on interferon-α/β receptor-1 blocking antibodies or the vaccinia virus B18R interferon decoy receptor to suppress innate immune responses and achieve effective transgene expression.[9,21,26,27] Similarly, corticosteroids have been used to enhance antigen expression by reducing saRNA-induced innate immune activation.[20] Here, we demonstrate that encoding broad-spectrum innate immune suppression directly within the saRNA obviates the need for additional immune-modulatory treatments, thereby reducing treatment complexity. Moreover, this strategy localizes

immune suppression to transfected cells, which should minimize the risks of off-target effects associated with systemic immune suppression.

Expressing multiple transgenes may also be a useful strategy for developing novel therapeutics. The NF-κB, TGF-β, and JAK/signal transducer and activator of transcription (STAT) pathways are central to the progression of osteoarthritis.[121–123] The srIκBα-Smad7-SOCS1 saRNA construct provides a novel strategy to simultaneously target these pathways: srIκBα inhibits NF-κB, Smad7 blocks TGF-β, and SOCS1 suppresses the JAK/STAT pathway. Each of these proteins has been independently studied as a treatment for osteoarthritis,[124–126] and their combination within a single construct could represent a synergistic strategy to enhance therapeutic efficacy. While arthritogenic alphaviruses such as chikungunya virus and Ross river virus can drive inflammatory responses in FLS, including upregulation of secreted proteolytic molecules such as matrix metalloproteases,[127,128] the lack of FAP-α upregulation in transfected FLS provides some evidence that saRNA transfection does not trigger comparable responses. Moreover, the reduction in basal FAP-α levels observed with the srIκBα and srIκBα-Smad7-SOCS1 constructs raises the possibility that saRNA could serve as a tool for suppressing fibroblast activation in inflammatory settings. This approach could hold therapeutic potential in arthritis treatment,[129] warranting further investigation in disease models.

In addition to expressing therapeutic transgenes, saRNA holds potential for inducing therapeutic effects by modulating translational control. While the strategy outlined in this report mitigated eIF2α phosphorylation, it was not effective at preventing saRNA-induced reductions in eIF4E phosphorylation. *In vitro* directed evolution of the RdRp replicon[6,24,130] may offer a potential solution to this challenge. Furthermore, we found that srIκBα expression decreased eIF4E levels, consistent with previous findings.[131] While reducing eIF4E activity through saRNA or srIκBα expression could lower transgene expression, it may also have therapeutic value, as lower eIF4E activity is associated with decreased pain sensitivity,[132] inhibition of tumorigenesis[133], improvement of neurodevelopmental social deficits[134], and increased longevity.[135] We also observed that srIκBα expression reduced phosphorylation of eIF2α, while the E3-NSs-L* construct reduced PKR levels. Given that eIF2α phosphorylation activates the integrated stress response, a pathway often driven by PKR in age-related diseases like neurodegeneration,[136] saRNA may represent a novel approach to modulate stress responses in these conditions.

Our findings present a fully saRNA-based strategy to address a key limitation of saRNA: replication driven innate immune stimulation. By inhibiting multiple innate immune pathways through proteins expressed via cap-independent translation, we mitigate the intrinsic cytotoxicity of saRNA. This approach enables sustained transgene expression with minimal cytotoxicity and antiviral cytokine release, all without the need for exogenous immunosuppressants. Given the established success of saRNA *in vivo*—including its application in preclinical models[6,18,22,26] and approved human vaccines[120,137]—we anticipate that this strategy will perform effectively *in vivo*, which future studies will address. This work advances the therapeutic potential of saRNA for non-immunotherapy applications, including protein replacement therapy, therapeutic antibody production, genome editing, cellular reprogramming, and immune cell engineering, where prolonged innate immune stimulation is undesirable. Importantly, the ability to externally regulate transgene expression offers precise control and serves as a critical safety mechanism for future clinical applications.

MATERIALS & METHODS

Experimental Design

This study aimed to develop and evaluate saRNA constructs that modulate innate immune responses, specifically targeting dsRNA sensing and inflammatory signaling pathways, to reduce saRNA-induced cytotoxicity, cytokine expression, and achieve sustained transgene expression. To this end, we engineered saRNA constructs that co-express multiple viral innate immune inhibitors and cellular inhibitors of inflammatory signaling. The constructs were designed to enable monitoring of cap-dependent and cap-independent translation using distinct fluorescent proteins.

The experimental approach included cloning the saRNA constructs using molecular biology techniques, followed by *in vitro* transcription and transfection into mouse primary FLS. Transfected cells were analyzed using fluorescence-based microplate assays to assess cell number, cell viability, phosphatidylserine exposure, and fluorescent protein expression. Further evaluations of translational control, FLS activation markers, RNA integrity, and cytokine secretion were conducted using in-cell western assays, capillary electrophoresis, and bead-based immunoassays. Finally, the ability to control saRNA transgene expression was explored using a small-molecule inhibitor targeting the VEEV RdRp.

Plasmid cloning and construct design

The commercially available TagGFP2 E3L Simplicon vector (SCR725, Merck) served as the saRNA backbone in this study. After removing the TagGFP2-IRES-E3 sequence, various constructs were generated by combining different elements using restriction digests (FastDigest, Thermo Scientific), overlap extension PCR (Phusion, Thermo Scientific), and HiFi assembly (NEBuilder, New England Biolabs).

Genetic elements were sourced as follows: mScarlet3 from pDx_mScarlet3 (a gift from Dorus Gadella [Addgene plasmid #189754]),[138] IRES-EGFP from pIRES2-EGFP (Clontech), and IRES-E3 and IRES-PuroR (puromycin resistance) from the original TagGFP2 E3L Simplicon vector.

Custom gene synthesis (GeneArt, Thermo Scientific) was used to produce IRES-moxBFP, IRES-E3-T2A-NSs-P2A-L*-E2A-mEGFP, and IRES-srIκBα-P2A-Smad7-T2A-SOCS1 sequences. The IRES sequence was derived from pIRES2-EGFP (Clontech). Other sequences were derived from public databases: moxBFP (FPbase ID: SSTDU),[139] mEGFP (FPbase ID: QKFJN), E3 (UniProt: P21605-1), NSs (UniProt: P21699), L* (UniProt: P0DJX4), Smad7 (UniProt: O35253-1), and SOCS1 (UniProt: O35716). srIκBα was engineered from IκBα (UniProt: Q9Z1E3) by substituting serines 32 and 36 with alanines. All synthesized sequences were codon-optimized for mouse expression (GenSmart, GenScript).

Plasmids were cloned in DH5α competent *Escherichia coli* (High Efficiency, New England Biolabs) and purified by maxiprep (PureLink HiPure, Invitrogen). All plasmid sequences were verified using nanopore whole plasmid sequencing (Plasmidsaurus).

RNA synthesis

Plasmids were linearized using XbaI (FastDigest, Thermo Scientific) at 37°C for 3 hours. The linear plasmids were purified by phenol-chloroform extraction followed by sodium acetate ethanol precipitation. Uncapped RNA was synthesized *in vitro* using the T7 RiboMAX Large Scale RNA Production kit (Promega) at 37°C for 2 hours. After purification by ammonium acetate precipitation, the RNA was denatured at 65°C for 5 minutes. Cap-1 structures were then generated using the Vaccinia Capping System in conjunction with mRNA cap 2'-O-methyltransferase (both from New England Biolabs) for 45 minutes at 37°C. Following another ammonium acetate purification, the RNA was treated with Antarctic phosphatase (New England Biolabs) for 30 minutes at 37°C. After a final ammonium acetate purification

step, the RNA was resuspended in THE RNA Storage Solution (Invitrogen), aliquoted, and stored at -80°C until use.

Animals

All mice used in this study were 5- to 12-week-old wildtype C57BL/6J mice (Bicester, UK). Both male and female mice were included, though sex differences in response to saRNA transfection were not analyzed. Mice were housed in groups of up to five in a temperature-controlled room (21°C), with bedding, a red shelter, and enrichment materials provided. They were maintained on a 12-hour light/dark cycle, with food and water available ad libitum. Mice were euthanized by exposure to CO_2 gas in a rising concentration, and death confirmed by dislocation of the atlanto-occipital joint by applying pressure to the side of the neck using thumb and forefinger, procedures in line with the Animals (Scientific Procedures) Act 1986 Amendment Regulations 2012.

Mouse primary FLS culture

We cultured FLS from mouse knee joints following established protocols,[140] with slight modifications. In brief, knee joints were exposed by cutting through the overlying skin with dissecting scissors. The patellar tendon was then grasped near the patella with Dumont tweezers, and spring scissors were used to sever the patellar tendon along with surrounding tissues. Finally, the patella was excised by cutting the quadriceps tendon, and excess muscle and tendons were carefully trimmed away.

Both patellae from each animal were collected into a microcentrifuge tube containing ice-cold sterile phosphate buffered saline (PBS), then transferred to a 24-well tissue culture plate (Costar) with FLS culture media. The media consisted of DMEM/F-12 (Invitrogen) supplemented with 25% fetal bovine serum (Sigma), 1X GlutaMAX (Gibco), and 100 µg/ml Primocin (InvivoGen).

The patellae were maintained in a humidified incubator at 37°C with 5% CO2, with media changes every 1-2 days. FLS outgrowth was observed, and after approximately 10 days, when cells reached 70% confluency, the patellae were transferred to new wells for further FLS collection. Cells attached to the original wells were passaged using 0.1% trypsin-EDTA (Sigma) into a single well of a 6-well plate (Costar). Cells were later expanded into T25 flasks (BioLite, Thermo Scientific or CELLSTAR, Greiner Bio-One) and passaged upon reaching confluency. After the second passage, Versene solution (Gibco) was used for cell dissociation.

FLS were used between passages 3 and 8. In most experiments, cells from the same animal were divided and plated onto 6-well or 24-well plates, allowing for parallel manipulations with matched conditions. Occasionally, when cell number was low, cells from different animals were pooled before division. Once plated for experiments, media was changed every 2-3 days.

Immunocytochemistry and confocal microscopy

Cells were plated on poly-D-lysine-coated glass-bottom 35 mm dishes (P35GC-1.5-14-C, MatTek) and fixed with 4% paraformaldehyde for 10 minutes at room temperature without permeabilization. After fixation, cells were washed twice with PBS, followed by blocking with 10% normal goat serum in PBS for 1 hour at room temperature.

Cells were then incubated overnight at 4°C in blocking buffer, either without primary antibody (no primary control) or with cadherin-11 (extracellular) rabbit polyclonal antibody (1:200, DF3523, Affinity Biosciences). After three washes with PBS, cells were incubated for 1 hour at room temperature in blocking buffer with 1 µg/ml Hoechst 33342, BioTracker NIR680 (1:2000, Merck), and goat anti-rabbit Alexa Fluor 488 secondary antibody (1:500, Invitrogen).

After four additional PBS washes, cells were imaged in PBS using a Leica Stellaris 5 confocal microscope equipped with a 40X oil immersion objective. Tile-scanned images were stitched using Las X microscopy software (Leica) to generate high-resolution panoramic images.

BioTracker staining

BioTracker NIR680 was diluted 1:2000 in unsupplemented DMEM/F-12. T25 flasks containing FLS were washed once with HBSS (with calcium and magnesium, Gibco), then incubated with the diluted dye for 30 minutes at 37°C. After incubation, the flasks were washed three times with FLS media, with each wash lasting 10 minutes at 37°C. The FLS were then dissociated using Versene and plated onto 6- or 24-well plates.

FLS transfection

For transfection in 6-well plates, the medium was removed and replaced with 1 ml of Opti-MEM I (Gibco). In a microcentrifuge tube, 500 ng of saRNA was diluted in 200 µl of Opti-MEM I. In a separate tube, 3 µl of Lipofectamine MessengerMAX (Invitrogen) was diluted in 100 µl of Opti-MEM I. After gently mixing, the complexes were incubated at room temperature for 5 minutes, then added dropwise to the cells. The cells were incubated with the complexes for 2 hours at 37°C, after which the media was removed and replaced with fresh FLS media. For transfection in 24-well plates, all volumes and amounts of saRNA were reduced fivefold.

Microplate imaging

Unless otherwise specified, black glass-bottom 6-well plates (P06-1.5H-N, Cellvis) were used for microplate imaging. Prior to imaging, the FLS media was replaced with Live Cell Imaging Solution (Invitrogen). Imaging was performed using the Odyssey M laser scanner (LI-COR), using LI-COR acquisition software with a plate offset of +1.45 mm and 100 µm resolution.

EGFP, mScarlet3, and BioTracker NIR680 were imaged using the 488, 520, and 700 channels, respectively. Spectral cross-excitation between EGFP and mScarlet3 in the 488 and 520 channels was corrected through linear unmixing analysis, as described below. Fluorescence intensity was quantified in ImageJ by measuring the integrated density within equal-area regions of interest for each well. Fluorescence values (EGFP, mScarlet3, and BioTracker) were normalized by the day 0 BioTracker signal measured before transfection to account for variations in starting cell number.

Linear unmixing analysis

saRNA constructs encoding individual fluorescent proteins (moxBFP, EGFP, or mScarlet3) were designed to assess cross-excitation among the fluorescent proteins used in this study. tSA201 cells (96121229, ECACC) were seeded in black glass-bottom 6-well plates coated with poly-D-lysine (Sigma) and transfected with the saRNA constructs. Cells were imaged the following day using an Odyssey M laser scanner, with fluorescence captured through the 488 and 520 channels. Expression of moxBFP was undetectable in both the 488 and 520 channels, and therefore it was excluded from further analysis. Bleed-through of EGFP into the 520 channel and mScarlet3 into the 488 channel was quantified using ImageJ, with cross-excitation determined to be 11.32% and 0.94%, respectively. The emission signals were assumed to be linearly proportional to the sum of the intensities of each fluorophore, and the unmixed EGFP and mScarlet3 signals were calculated using Python.

Annexin V assay

FLS were stained with BioTracker NIR680 and plated on black glass-bottom 24-well plates (Sensoplate, Greiner Bio-One). Cells were transfected with saRNA or treated with 0.5 μM staurosporine (Cayman Chemical) as a positive control.

Annexin V-CF800 conjugate (Biotium) was diluted to 250 ng/ml in Live Cell Imaging Solution (Invitrogen). On each day of the assay, wells were washed with Live Cell Imaging Solution and replaced with diluted Annexin V-CF800 solution. Plates were incubated at 37°C for 15 minutes. Following incubation, plates were washed 3 times with Live Cell Imaging Solution before imaging the 700 and 800 channels with an Odyssey M imager set to +1.45 mm image offset and 100 μm resolution.

Image analysis was performed using ImageJ. To correct for unidirectional spectral bleed-through of BioTracker NIR680 into the 800-channel, subtractive compensation was applied by dividing the 700-channel image by a factor of 800 and then subtracting it from the 800-channel image. Due to the presence of a small number of high-intensity speckles in the 800-channel image, area rather than fluorescence intensity was quantified. The display range of the 800-channel image was set between 0.25 and 2.5 and the image was thresholded using the method of Li.[141] The area of thresholded pixels within each well was then quantified and adjusted based on the BioTracker signal before transfection to account for variations in cell number. Data was then normalized to the average of the mock transfection condition.

Calcein AM staining

Calcein AM (Invitrogen) staining was performed according to the manufacturer's protocol. Briefly, cells were washed with HBSS and incubated with 2 μM calcein AM (diluted in HBSS) at 37°C for 30 minutes. Following three washes, cells were imaged in Live Cell Imaging Solution, and the 488-channel image was captured using an Odyssey M imager.

Although calcein AM and EGFP share overlapping spectra, calcein AM fluorescence was typically much higher than EGFP, making EGFP's contribution to the measured Calcein AM signal negligible in most cases. However, when the E3 construct was used, EGFP expression was sufficient to interfere with the signal. To address this, in experiments that included use of the E3 construct, a 488-channel image was captured prior to calcein AM application and subtracted from the post-application image to accurately measure calcein AM fluorescence.

Fluorescence intensity was quantified using ImageJ. In experiments where BioTracker was used, fluorescence values were corrected by the pre-transfection BioTracker signal to account for differences in starting cell number.

In-cell western assay

Cells were plated on black, glass-bottom 24-well plates. Alongside mock and saRNA transfections, one well was reserved for background subtraction, which received no treatment. Unless specified otherwise, experiments were conducted 2 days post-transfection. Cells were fixed with 4% paraformaldehyde for 10 minutes at room temperature, followed by two washes with tris-buffered saline (TBS). Permeabilization was then performed using 0.1% Triton X-100 in TBS for 10 minutes, followed by two additional TBS washes. After permeabilization, cells were blocked with Intercept TBS Blocking Buffer (LI-COR) for 1 hour at room temperature with gentle agitation.

Primary antibodies were diluted in Intercept Blocking Buffer and incubated with the cells overnight at 4°C. The background subtraction well was incubated with blocking buffer alone, without primary antibodies. The following primary antibodies were used: Phospho-eIF2α (Ser51) (D9G8) XP rabbit monoclonal (1:200, #3398, Cell Signaling Technology), eIF2α (L57A5) mouse monoclonal (1:200, #2103, Cell Signaling Technology), PKR rabbit polyclonal (1:500, #18244-1-AP, Proteintech), Phospho-eIF4E (S209)

rabbit monoclonal (1:200, #ab76256, Abcam), eIF4E mouse monoclonal (5D11) (1:200, #MA1-089, Invitrogen), and fibroblast activation protein (73.3) mouse monoclonal (20 µg/ml, #BE0374, InVivoMAb). Except for the fibroblast activation protein antibody, which was conjugated to DyLight 800 using the manufacturer's DyLight Antibody Labeling Kit (#53062, Thermo Scientific), all primary antibodies were unconjugated.

After washing the wells three times with TBS, cells were incubated for 1 hour at room temperature with the appropriate secondary antibodies or normalization stain, with gentle agitation. The secondary antibodies used were goat anti-mouse IRDye 800CW (1:800), donkey anti-rabbit IRDye 800CW (1:800), donkey anti-mouse IRDye 680RD (1:800), and CellTag 700 (1:500), all from LI-COR. The background subtraction well received secondary antibody but no CellTag. Following four additional washes with TBS, the plate was inverted and gently tapped on absorbent paper to remove excess liquid. The plate was then imaged using the Odyssey M imager with LI-COR Acquisition software using a plate offset of +1.45 and 100 µm resolution. Signal quantification was carried out using Empiria Studio software (LI-COR).

rRNA integrity analysis

FLS were plated in 6-well plates and either transfected with saRNA or subjected to mock transfection. After 26-30 hours (allowing for saRNA replication but before substantial cell loss), cells were harvested by scraping in 350 µl RLT buffer (QIAGEN) supplemented with 10 µl/ml β-mercaptoethanol (Sigma). Cell lysates were homogenized using QIAshredder columns (QIAGEN), and total RNA was extracted using the RNeasy Mini Kit (QIAGEN) according to the manufacturer's instructions. RNA quantity and quality were initially assessed using a N60 nanophotometer (Implen). Samples were aliquoted and stored at -80°C until further analysis. For detailed quality assessment, samples were transported on dry ice and analyzed using the RNA Pico Kit on the 2100 Bioanalyzer system (Agilent), performed by Cambridge Genomic Services. RNA Integrity Number (RIN) values were determined for each sample.

Bead-based immunoassay

FLS were stained with BioTracker and seeded onto 6-well plates. After transfection, the saRNA-lipofectamine complexes were replaced with 2 ml of fresh FLS media. Two days later, supernatants were collected and stored at -80°C until analysis. On the day of analysis, the supernatant was thawed on ice, and levels of 13 innate immune-related cytokines (IFN-γ, CXCL1, TNF-α, MCP-1, IL-12p70, CCL5, IL-1β, CXCL10, GM-CSF, IL-10, IFN-β, IFN-α, and IL-6) were measured using the LEGENDplex Mouse Anti-Virus Response Panel (740621, BioLegend) following the manufacturer's protocol. Samples were run in duplicate. A custom 3D-printed PETG vacuum manifold (designed with Fusion 360) was used for vacuum filtration, and beads were analyzed using a CytoPLEX LX flow cytometer (Beckman Coulter). Data analysis was performed with the LEGENDplex Qognit Data Analysis Suite (BioLegend). To account for differences in cell number between wells, cytokine levels were corrected based on the BioTracker signal before transfection.

ML336 experiments

ML336 (Cayman Chemical) was dissolved in DMSO (Sigma) at a stock concentration of 10 mM, and aliquots were stored at -20°C. For treatments, ML336 was added to cell cultures at a final concentration of 1 µM, while vehicle control cultures received 0.01% DMSO.

Statistical Analysis

All statistical analyses were conducted using GraphPad Prism 9, with specific tests detailed in the corresponding figure legends. All statistical tests were two-sided tests.

DATA AVAILABILITY STATEMENT

The code for the unmixing analysis is available at https://github.com/lariferg/spectral_unmixing.

The 3D printed vacuum manifold compatible with the LEGENDplex assay has been deposited in the NIH 3D print exchange (3DPX-021388).

All data needed to evaluate the conclusions in the paper are present in the paper, the Supplementary Materials, and the Figshare repository http://doi.org/10.6084/m9.figshare.27091972.

ACKNOWLEDGMENTS

The authors gratefully acknowledge the Cambridge Advanced Imaging Centre, the flow cytometry facility from the School of the Biological Sciences, and Cambridge Genomic Services for their support & assistance in this work. The authors would like to thank Dr. Paul Miller for providing the pDx_mScarlet3 plasmid and Dr. Alex Cloake for providing the pIRES2-EGFP plasmid used in this study. T.K.L. acknowledges support from a Horizon Europe Marie Skłodowska-Curie Actions European Postdoctoral Fellowship (UKRI Guarantee) [EP/X023117/1]. A.R. and L.W.P. disclose support from AstraZeneca PhD studentships [G115018 and G113502, respectively]. L.F. discloses support from funding provided by the MRC Postdoctoral Training Scheme. E.St.J.S. acknowledges funding from the UKRI and Versus Arthritis [MR/W002426/1] as part of the ADVANTAGE visceral pain consortium through the Advanced Pain Discovery Platform (APDP) and the Wellcome Trust [225856/Z/22/Z].

AUTHOR CONTRIBUTIONS

Conceptualization, T.K.L. and E.St.J.S
Formal analysis: T.K.L., E.St.J.S.
Funding acquisition: E.St.J.S., T.K.L.
Investigation: T.K.L., A.R., L.W.P.
Methodology: T.K.L., T.A.
Resources: E.St.J.S., T.K.L.
Software: L.F.
Supervision: E.St.J.S., T.K.L.
Visualisation: T.K.L., E.St.J.S.
Writing—original draft: T.K.L.
Writing—reviewing & editing: E.St.J.S., L.F.

DECLARATION OF INTERESTS

Authors declare that they have no competing interests.

KEYWORDS

Self-amplifying RNA, alphavirus vectors, RNA replicons, fibroblast-like synoviocytes, double-stranded RNA sensors, nuclear factor kappa B, viral innate immune antagonists, RNA vaccines, RNA therapeutics, gene therapy

DECLARATION OF GENERATIVE AI AND AI-ASSISTED TECHNOLOGIES IN THE WRITING PROCESS

During the preparation of this work, the authors used OpenAI's ChatGPT to enhance clarity and flow of the writing. After using this tool, the authors reviewed and edited the content as needed and take full responsibility for the content of the publication.

REFERENCES

1. Frolov, I., Hoffman, T.A., Prágai, B.M., Dryga, S.A., Huang, H.V., Schlesinger, S., and Rice, C.M. (1996). Alphavirus-based expression vectors: strategies and applications. Proc Natl Acad Sci U S A *93*, 11371–11377.

2. Bloom, K., van den Berg, F., and Arbuthnot, P. (2021). Self-amplifying RNA vaccines for infectious diseases. Gene Ther *28*, 117–129. https://doi.org/10.1038/s41434-020-00204-y.

3. Pietilä, M.K., Hellström, K., and Ahola, T. (2017). Alphavirus polymerase and RNA replication. Virus Research *234*, 44–57. https://doi.org/10.1016/j.virusres.2017.01.007.

4. Maruggi, G., Zhang, C., Li, J., Ulmer, J.B., and Yu, D. (2019). mRNA as a Transformative Technology for Vaccine Development to Control Infectious Diseases. Mol Ther *27*, 757–772. https://doi.org/10.1016/j.ymthe.2019.01.020.

5. Akhrymuk, I., Frolov, I., and Frolova, E.I. (2016). Both RIG-I and MDA5 detect alphavirus replication in concentration-dependent mode. Virology *487*, 230–241. https://doi.org/10.1016/j.virol.2015.09.023.

6. Gong, Y., Yong, D., Liu, G., Xu, J., Ding, J., and Jia, W. (2024). A Novel Self-Amplifying mRNA with Decreased Cytotoxicity and Enhanced Protein Expression by Macrodomain Mutations. Advanced Science *n/a*, 2402936. https://doi.org/10.1002/advs.202402936.

7. Gorchakov, R., Frolova, E., Williams, B.R.G., Rice, C.M., and Frolov, I. (2004). PKR-Dependent and -Independent Mechanisms Are Involved in Translational Shutoff during Sindbis Virus Infection. Journal of Virology *78*, 8455–8467. https://doi.org/10.1128/jvi.78.16.8455-8467.2004.

8. Dominguez, F., Palchevska, O., Frolova, E.I., and Frolov, I. (2023). Alphavirus-based replicons demonstrate different interactions with host cells and can be optimized to increase protein expression. Journal of Virology *97*, e01225-23. https://doi.org/10.1128/jvi.01225-23.

9. Vanluchene, H., Gillon, O., Peynshaert, K., De Smedt, S.C., Sanders, N., Raemdonck, K., and Remaut, K. (2024). Less is more: Self-amplifying mRNA becomes self-killing upon dose escalation in immune-competent retinal cells. European Journal of Pharmaceutics and Biopharmaceutics *196*, 114204. https://doi.org/10.1016/j.ejpb.2024.114204.

10. Frolov, I., and Schlesinger, S. (1994). Comparison of the effects of Sindbis virus and Sindbis virus replicons on host cell protein synthesis and cytopathogenicity in BHK cells. J Virol *68*, 1721–1727. https://doi.org/10.1128/jvi.68.3.1721-1727.1994.

1000 11. Terenzi, F., deVeer, M.J., Ying, H., Restifo, N.P., Williams, B.R., and Silverman, R.H. (1999). The
1001 antiviral enzymes PKR and RNase L suppress gene expression from viral and non-viral based vectors.
1002 Nucleic Acids Res *27*, 4369–4375. https://doi.org/10.1093/nar/27.22.4369.

1003 12. Li, Y., Su, Z., Zhao, W., Zhang, X., Momin, N., Zhang, C., Wittrup, K.D., Dong, Y., Irvine, D.J., and
1004 Weiss, R. (2020). Multifunctional oncolytic nanoparticles deliver self-replicating IL-12 RNA to
1005 eliminate established tumors and prime systemic immunity. Nat Cancer *1*, 882–893.
1006 https://doi.org/10.1038/s43018-020-0095-6.

1007 13. Venticinque, L., and Meruelo, D. (2010). Sindbis viral vector induced apoptosis requires translational
1008 inhibition and signaling through Mcl-1 and Bak. Mol Cancer *9*, 37. https://doi.org/10.1186/1476-
1009 4598-9-37.

1010 14. Mastrangelo, A.J., Hardwick, J.M., Bex, F., and Betenbaugh, M.J. (2000). Part I. Bcl-2 and Bcl-x(L)
1011 limit apoptosis upon infection with alphavirus vectors. Biotechnol Bioeng *67*, 544–554.

1012 15. Frolov, I., Agapov, E., Thomas A Hoffman, J., Prágai, B.M., Lippa, M., Schlesinger, S., and Rice, C.M.
1013 (1999). Selection of RNA Replicons Capable of Persistent Noncytopathic Replication in Mammalian
1014 Cells. Journal of Virology *73*, 3854. https://doi.org/10.1128/jvi.73.5.3854-3865.1999.

1015 16. Lundstrom, K., Abenavoli, A., Malgaroli, A., and Ehrengruber, M.U. (2003). Novel semliki forest virus
1016 vectors with reduced cytotoxicity and temperature sensitivity for long-term enhancement of
1017 transgene expression. Molecular Therapy *7*, 202–209. https://doi.org/10.1016/S1525-
1018 0016(02)00056-4.

1019 17. Pepini, T., Pulichino, A.-M., Carsillo, T., Carlson, A.L., Sari-Sarraf, F., Ramsauer, K., Debasitis, J.C.,
1020 Maruggi, G., Otten, G.R., Geall, A.J., et al. (2017). Induction of an IFN-Mediated Antiviral Response
1021 by a Self-Amplifying RNA Vaccine: Implications for Vaccine Design. The Journal of Immunology *198*,
1022 4012–4024. https://doi.org/10.4049/jimmunol.1601877.

1023 18. Blakney, A.K., McKay, P.F., Bouton, C.R., Hu, K., Samnuan, K., and Shattock, R.J. (2021). Innate
1024 Inhibiting Proteins Enhance Expression and Immunogenicity of Self-Amplifying RNA. Mol Ther *29*,
1025 1174–1185. https://doi.org/10.1016/j.ymthe.2020.11.011.

1026 19. McGee, J.E., Kirsch, J.R., Kenney, D., Cerbo, F., Chavez, E.C., Shih, T.-Y., Douam, F., Wong, W.W., and
1027 Grinstaff, M.W. (2024). Complete substitution with modified nucleotides in self-amplifying RNA
1028 suppresses the interferon response and increases potency. Nat Biotechnol, 1–7.
1029 https://doi.org/10.1038/s41587-024-02306-z.

1030 20. Zhong, Z., McCafferty, S., Opsomer, L., Wang, H., Huysmans, H., De Temmerman, J., Lienenklaus, S.,
1031 Portela Catani, J.P., Combes, F., and Sanders, N.N. (2021). Corticosteroids and cellulose purification
1032 improve, respectively, the in vivo translation and vaccination efficacy of sa-mRNAs. Molecular
1033 Therapy *29*, 1370–1381. https://doi.org/10.1016/j.ymthe.2021.01.023.

1034 21. Yoshioka, N., Gros, E., Li, H.-R., Kumar, S., Deacon, D.C., Maron, C., Muotri, A.R., Chi, N.C., Fu, X.-D.,
1035 Yu, B.D., et al. (2013). Efficient Generation of Human iPS Cells by a Synthetic Self-Replicative RNA.
1036 Cell Stem Cell *13*, 10.1016/j.stem.2013.06.001. https://doi.org/10.1016/j.stem.2013.06.001.

1037 22. Beissert, T., Koste, L., Perkovic, M., Walzer, K.C., Erbar, S., Selmi, A., Diken, M., Kreiter, S., Türeci, Ö.,
1038 and Sahin, U. (2017). Improvement of In Vivo Expression of Genes Delivered by Self-Amplifying RNA
1039 Using Vaccinia Virus Immune Evasion Proteins. Hum Gene Ther *28*, 1138–1146.
1040 https://doi.org/10.1089/hum.2017.121.

1041 23. Xue, Y., Zhang, Y., Zhong, Y., Du, S., Hou, X., Li, W., Li, H., Wang, S., Wang, C., Yan, J., et al. (2024).
1042 LNP-RNA-engineered adipose stem cells for accelerated diabetic wound healing. Nat Commun *15*,
1043 739. https://doi.org/10.1038/s41467-024-45094-5.

1044 24. Li, Y., Teague, B., Zhang, Y., Su, Z., Porter, E., Dobosh, B., Wagner, T., Irvine, D.J., and Weiss, R.
1045 (2019). In vitro evolution of enhanced RNA replicons for immunotherapy. Sci Rep *9*, 6932.
1046 https://doi.org/10.1038/s41598-019-43422-0.

1047 25. Blakney, A.K., Ip, S., and Geall, A.J. (2021). An Update on Self-Amplifying mRNA Vaccine
1048 Development. Vaccines (Basel) *9*, 97. https://doi.org/10.3390/vaccines9020097.

1049 26. Erasmus, J.H., Archer, J., Fuerte-Stone, J., Khandhar, A.P., Voigt, E., Granger, B., Bombardi, R.G.,
1050 Govero, J., Tan, Q., Durnell, L.A., et al. (2020). Intramuscular Delivery of Replicon RNA Encoding
1051 ZIKV-117 Human Monoclonal Antibody Protects against Zika Virus Infection. Molecular Therapy
1052 Methods & Clinical Development *18*, 402–414. https://doi.org/10.1016/j.omtm.2020.06.011.

1053 27. Kim, Y.G., Baltabekova, A.Z., Zhiyenbay, E.E., Aksambayeva, A.S., Shagyrova, Z.S., Khannanov, R.,
1054 Ramanculov, E.M., and Shustov, A.V. (2017). Recombinant Vaccinia virus-coded interferon inhibitor
1055 B18R: Expression, refolding and a use in a mammalian expression system with a RNA-vector. PLOS
1056 ONE *12*, e0189308. https://doi.org/10.1371/journal.pone.0189308.

1057 28. Merrick, W.C. (2004). Cap-dependent and cap-independent translation in eukaryotic systems. Gene
1058 *332*, 1–11. https://doi.org/10.1016/j.gene.2004.02.051.

1059 29. Yang, Y., and Wang, Z. (2019). IRES-mediated cap-independent translation, a path leading to hidden
1060 proteome. Journal of Molecular Cell Biology *11*, 911–919. https://doi.org/10.1093/jmcb/mjz091.

1061 30. Maglaviceanu, A., Wu, B., and Kapoor, M. (2021). Fibroblast-like synoviocytes: Role in synovial
1062 fibrosis associated with osteoarthritis. Wound Repair and Regeneration *29*, 642–649.
1063 https://doi.org/10.1111/wrr.12939.

1064 31. Mousavi, M.J., Karami, J., Aslani, S., Tahmasebi, M.N., Vaziri, A.S., Jamshidi, A., Farhadi, E., and
1065 Mahmoudi, M. (2021). Transformation of fibroblast-like synoviocytes in rheumatoid arthritis; from a
1066 friend to foe. Autoimmun Highlights *12*, 3. https://doi.org/10.1186/s13317-020-00145-x.

1067 32. Honig, M.G., and Hume, R.I. (1986). Fluorescent carbocyanine dyes allow living neurons of identified
1068 origin to be studied in long-term cultures. J Cell Biol *103*, 171–187.
1069 https://doi.org/10.1083/jcb.103.1.171.

1070 33. Bertrand, R., Solary, E., O'Connor, P., Kohn, K.W., and Pommier, Y. (1994). Induction of a Common
1071 Pathway of Apoptosis by Staurosporine. Experimental Cell Research *211*, 314–321.
1072 https://doi.org/10.1006/excr.1994.1093.

1073 34. Rehwinkel, J., and Gack, M.U. (2020). RIG-I-like receptors: their regulation and roles in RNA sensing.
1074 Nat Rev Immunol *20*, 537–551. https://doi.org/10.1038/s41577-020-0288-3.

1075 35. Junior, A.G.D., Sampaio, N.G., and Rehwinkel, J. (2019). A Balancing Act: MDA5 in Antiviral Immunity
1076 and Autoinflammation. Trends in Microbiology *27*, 75–85.
1077 https://doi.org/10.1016/j.tim.2018.08.007.

1078 36. Gal-Ben-Ari, S., Barrera, I., Ehrlich, M., and Rosenblum, K. (2019). PKR: A Kinase to Remember.
1079 Front. Mol. Neurosci. *11*. https://doi.org/10.3389/fnmol.2018.00480.

1080 37. Silverman, R.H. (2007). Viral Encounters with 2′,5′-Oligoadenylate Synthetase and RNase L during
1081 the Interferon Antiviral Response. Journal of Virology *81*, 12720–12729.
1082 https://doi.org/10.1128/jvi.01471-07.

1083 38. Szczerba, M., Subramanian, S., Trainor, K., McCaughan, M., Kibler, K.V., and Jacobs, B.L. (2022).
1084 Small Hero with Great Powers: Vaccinia Virus E3 Protein and Evasion of the Type I IFN Response.
1085 Biomedicines *10*, 235. https://doi.org/10.3390/biomedicines10020235.

1086 39. Kalveram, B., and Ikegami, T. (2013). Toscana Virus NSs Protein Promotes Degradation of Double-
1087 Stranded RNA-Dependent Protein Kinase. J Virol *87*, 3710–3718. https://doi.org/10.1128/JVI.02506-
1088 12.

1089 40. Drappier, M., Jha, B.K., Stone, S., Elliott, R., Zhang, R., Vertommen, D., Weiss, S.R., Silverman, R.H.,
1090 and Michiels, T. (2018). A novel mechanism of RNase L inhibition: Theiler's virus L* protein prevents
1091 2-5A from binding to RNase L. PLoS Pathog *14*, e1006989.
1092 https://doi.org/10.1371/journal.ppat.1006989.

1093 41. Liu, Z., Chen, O., Wall, J.B.J., Zheng, M., Zhou, Y., Wang, L., Ruth Vaseghi, H., Qian, L., and Liu, J.
1094 (2017). Systematic comparison of 2A peptides for cloning multi-genes in a polycistronic vector. Sci
1095 Rep *7*, 2193. https://doi.org/10.1038/s41598-017-02460-2.

1096 42. Costigan, A., Hollville, E., and Martin, S.J. (2023). Discriminating Between Apoptosis, Necrosis,
1097 Necroptosis, and Ferroptosis by Microscopy and Flow Cytometry. Current Protocols *3*, e951.
1098 https://doi.org/10.1002/cpz1.951.

1099 43. Liu, Q., Huang, J., Xia, J., Liang, Y., and Li, G. (2022). Tracking tools of extracellular vesicles for
1100 biomedical research. Front. Bioeng. Biotechnol. *10*. https://doi.org/10.3389/fbioe.2022.943712.

1101 44. Chiaradia, E., Tancini, B., Emiliani, C., Delo, F., Pellegrino, R.M., Tognoloni, A., Urbanelli, L., and
1102 Buratta, S. (2021). Extracellular Vesicles under Oxidative Stress Conditions: Biological Properties and
1103 Physiological Roles. Cells *10*, 1763. https://doi.org/10.3390/cells10071763.

1104 45. van Genderen, H., Kenis, H., Lux, P., Ungeth, L., Maassen, C., Deckers, N., Narula, J., Hofstra, L., and
1105 Reutelingsperger, C. (2006). In vitro measurement of cell death with the annexin A5 affinity assay.
1106 Nat Protoc *1*, 363–367. https://doi.org/10.1038/nprot.2006.55.

1107 46. Crowley, L.C., Marfell, B.J., Scott, A.P., and Waterhouse, N.J. (2016). Quantitation of Apoptosis and
1108 Necrosis by Annexin V Binding, Propidium Iodide Uptake, and Flow Cytometry. Cold Spring Harb
1109 Protoc *2016*. https://doi.org/10.1101/pdb.prot087288.

1110 47. Chan, L.L., Wilkinson, A.R., Paradis, B.D., and Lai, N. (2012). Rapid Image-based Cytometry for
1111 Comparison of Fluorescent Viability Staining Methods. J Fluoresc *22*, 1301–1311.
1112 https://doi.org/10.1007/s10895-012-1072-y.

1113 48. Baird, T.D., and Wek, R.C. (2012). Eukaryotic Initiation Factor 2 Phosphorylation and Translational
1114 Control in Metabolism. Advances in Nutrition *3*, 307. https://doi.org/10.3945/an.112.002113.

1115 49. Mars, J.-C., Culjkovic-Kraljacic, B., and Borden, K.L.B. (2024). eIF4E orchestrates mRNA processing,
1116 RNA export and translation to modify specific protein production. Nucleus *15*, 2360196.
1117 https://doi.org/10.1080/19491034.2024.2360196.

1118 50. Burke, J.M., Moon, S.L., Matheny, T., and Parker, R. (2019). RNase L Reprograms Translation by
1119 Widespread mRNA Turnover Escaped by Antiviral mRNAs. Molecular Cell *75*, 1203-1217.e5.
1120 https://doi.org/10.1016/j.molcel.2019.07.029.

1121 51. Burke, J.M., Gilchrist, A.R., Sawyer, S.L., and Parker, R. (2021). RNase L limits host and viral protein
1122 synthesis via inhibition of mRNA export. Science Advances *7*, eabh2479.
1123 https://doi.org/10.1126/sciadv.abh2479.

1124 52. Donovan, J., Rath, S., Kolet-Mandrikov, D., and Korennykh, A. (2017). Rapid RNase L-driven arrest of
1125 protein synthesis in the dsRNA response without degradation of translation machinery. RNA *23*,
1126 1660–1671. https://doi.org/10.1261/rna.062000.117.

1127 53. Whelan, J.N., Li, Y., Silverman, R.H., and Weiss, S.R. (2019). Zika Virus Production Is Resistant to
1128 RNase L Antiviral Activity. J Virol *93*, e00313-19. https://doi.org/10.1128/JVI.00313-19.

1129 54. Paul, D., and Bartenschlager, R. (2013). Architecture and biogenesis of plus-strand RNA virus
1130 replication factories. World J Virol *2*, 32–48. https://doi.org/10.5501/wjv.v2.i2.32.

1131 55. Silverman, R.H. (2007). Viral encounters with 2',5'-oligoadenylate synthetase and RNase L during the
1132 interferon antiviral response. J Virol *81*, 12720–12729. https://doi.org/10.1128/JVI.01471-07.

1133 56. Schroeder, A., Mueller, O., Stocker, S., Salowsky, R., Leiber, M., Gassmann, M., Lightfoot, S., Menzel,
1134 W., Granzow, M., and Ragg, T. (2006). The RIN: an RNA integrity number for assigning integrity
1135 values to RNA measurements. BMC Molecular Biology *7*, 3. https://doi.org/10.1186/1471-2199-7-3.

1136 57. Karasik, A., Jones, G.D., DePass, A.V., and Guydosh, N.R. (2021). Activation of the antiviral factor
1137 RNase L triggers translation of non-coding mRNA sequences. Nucleic Acids Research *49*, 6007–6026.
1138 https://doi.org/10.1093/nar/gkab036.

1139 58. Santoro, M.G., Rossi, A., and Amici, C. (2003). NF-κB and virus infection: who controls whom. The
1140 EMBO Journal *22*, 2552–2560. https://doi.org/10.1093/emboj/cdg267.

1141 59. Mitchell, J.P., and Carmody, R.J. (2018). Chapter Two - NF-κB and the Transcriptional Control of
1142 Inflammation. In International Review of Cell and Molecular Biology Transcriptional Gene Regulation
1143 in Health and Disease., F. Loos, ed. (Academic Press), pp. 41–84.
1144 https://doi.org/10.1016/bs.ircmb.2017.07.007.

1145 60. Lee, Y.-R., Kweon, S.-H., Kwon, K.-B., Park, J.-W., Yoon, T.-R., and Park, B.-H. (2009). Inhibition of IL-
1146 1β-mediated inflammatory responses by the IκBα super-repressor in human fibroblast-like
1147 synoviocytes. Biochemical and Biophysical Research Communications *378*, 90–94.
1148 https://doi.org/10.1016/j.bbrc.2008.11.002.

1149 61. Brown, K., Gerstberger, S., Carlson, L., Franzoso, G., and Siebenlist, U. (1995). Control of IκB-α
1150 Proteolysis by Site-Specific, Signal-Induced Phosphorylation. Science *267*, 1485–1488.
1151 https://doi.org/10.1126/science.7878466.

1152 62. Yan, X., Liu, Z., and Chen, Y. (2009). Regulation of TGF-β signaling by Smad7. Acta Biochimica et
1153 Biophysica Sinica *41*, 263–272. https://doi.org/10.1093/abbs/gmp018.

1154 63. Sobah, M.L., Liongue, C., and Ward, A.C. (2021). SOCS Proteins in Immunity, Inflammatory Diseases,
1155 and Immune-Related Cancer. Front Med (Lausanne) *8*, 727987.
1156 https://doi.org/10.3389/fmed.2021.727987.

1157 64. Dimitriou, I.D., Clemenza, L., Scotter, A.J., Chen, G., Guerra, F.M., and Rottapel, R. (2008). Putting
1158 out the fire: coordinated suppression of the innate and adaptive immune systems by SOCS1 and
1159 SOCS3 proteins. Immunological Reviews *224*, 265–283. https://doi.org/10.1111/j.1600-
1160 065X.2008.00659.x.

1161 65. Blumer, T., Coto-Llerena, M., Duong, F.H.T., and Heim, M.H. (2017). SOCS1 is an inducible negative
1162 regulator of interferon λ (IFN-λ)-induced gene expression in vivo. J Biol Chem *292*, 17928–17938.
1163 https://doi.org/10.1074/jbc.M117.788877.

1164 66. Bauer, S., Jendro, M.C., Wadle, A., Kleber, S., Stenner, F., Dinser, R., Reich, A., Faccin, E., Gödde, S.,
1165 Dinges, H., et al. (2006). Fibroblast activation protein is expressed by rheumatoid myofibroblast-like
1166 synoviocytes. Arthritis Res Ther *8*, R171. https://doi.org/10.1186/ar2080.

1167 67. Zhang, H.E., Hamson, E.J., Koczorowska, M.M., Tholen, S., Chowdhury, S., Bailey, C.G., Lay, A.J.,
1168 Twigg, S.M., Lee, Q., Roediger, B., et al. (2019). Identification of Novel Natural Substrates of
1169 Fibroblast Activation Protein-alpha by Differential Degradomics and Proteomics. Mol Cell
1170 Proteomics *18*, 65–85. https://doi.org/10.1074/mcp.RA118.001046.

1171 68. Fan, A., Wu, G., Wang, J., Lu, L., Wang, J., Wei, H., Sun, Y., Xu, Y., Mo, C., Zhang, X., et al. (2023).
1172 Inhibition of fibroblast activation protein ameliorates cartilage matrix degradation and osteoarthritis
1173 progression. Bone Res *11*, 1–12. https://doi.org/10.1038/s41413-022-00243-8.

1174 69. Croft, A.P., Campos, J., Jansen, K., Turner, J.D., Marshall, J., Attar, M., Savary, L., Wehmeyer, C.,
1175 Naylor, A.J., Kemble, S., et al. (2019). Distinct fibroblast subsets drive inflammation and damage in
1176 arthritis. Nature *570*, 246–251. https://doi.org/10.1038/s41586-019-1263-7.

1177 70. Boyd, D.F., Allen, E.K., Randolph, A.G., Guo, X.J., Weng, Y., Sanders, C.J., Bajracharya, R., Lee, N.K.,
1178 Guy, C.S., Vogel, P., et al. (2020). Exuberant fibroblast activity compromises lung function via
1179 ADAMTS-4. Nature *587*, 466–471. https://doi.org/10.1038/s41586-020-2877-5.

1180 71. Krausgruber, T., Fortelny, N., Fife-Gernedl, V., Senekowitsch, M., Schuster, L.C., Lercher, A., Nemc,
1181 A., Schmidl, C., Rendeiro, A.F., Bergthaler, A., et al. (2020). Structural cells are key regulators of

1182 organ-specific immune response. Nature *583*, 296–302. https://doi.org/10.1038/s41586-020-2424-
1183 4.

1184 72. Nagata, L.P., Wong, J.P., Hu, W., and Wu, J.Q. (2013). Vaccines and Therapeutics for the Encephalitic
1185 Alphaviruses. Future Virology *8*, 661–674. https://doi.org/10.2217/fvl.13.42.

1186 73. Chung, D., Schroeder, C.E., Sotsky, J., Yao, T., Roy, S., Smith, R.A., Tower, N.A., Noah, J.W., McKellip,
1187 S., Sosa, M., et al. (2010). ML336: Development of Quinazolinone-Based Inhibitors Against
1188 Venezuelan Equine Encephalitis Virus (VEEV). In Probe Reports from the NIH Molecular Libraries
1189 Program (National Center for Biotechnology Information (US)).

1190 74. Minnaert, A.-K., Vanluchene, H., Verbeke, R., Lentacker, I., De Smedt, S.C., Raemdonck, K., Sanders,
1191 N.N., and Remaut, K. (2021). Strategies for controlling the innate immune activity of conventional
1192 and self-amplifying mRNA therapeutics: Getting the message across. Adv Drug Deliv Rev *176*,
1193 113900. https://doi.org/10.1016/j.addr.2021.113900.

1194 75. Frolova, E.I., Palchevska, O., Dominguez, F., and Frolov, I. Alphavirus-induced transcriptional and
1195 translational shutoffs play major roles in blocking the formation of stress granules. J Virol *97*,
1196 e00979-23. https://doi.org/10.1128/jvi.00979-23.

1197 76. Berglund, P., Finzi, D., Bennink, J.R., and Yewdell, J.W. (2007). Viral Alteration of Cellular
1198 Translational Machinery Increases Defective Ribosomal Products. Journal of Virology *81*, 7220–
1199 7229. https://doi.org/10.1128/jvi.00137-07.

1200 77. Fros, J.J., and Pijlman, G.P. (2016). Alphavirus Infection: Host Cell Shut-Off and Inhibition of Antiviral
1201 Responses. Viruses *8*, 166. https://doi.org/10.3390/v8060166.

1202 78. Fernandez, J., Yaman, I., Sarnow, P., Snider, M.D., and Hatzoglou, M. (2002). Regulation of Internal
1203 Ribosomal Entry Site-mediated Translation by Phosphorylation of the Translation Initiation Factor
1204 eIF2α*. Journal of Biological Chemistry *277*, 19198–19205.
1205 https://doi.org/10.1074/jbc.M201052200.

1206 79. Scheper, G.C., and Proud, C.G. (2002). Does phosphorylation of the cap-binding protein eIF4E play a
1207 role in translation initiation? European Journal of Biochemistry *269*, 5350–5359.
1208 https://doi.org/10.1046/j.1432-1033.2002.03291.x.

1209 80. Dyer, J.R., Michel, S., Lee, W., Castellucci, V.F., Wayne, N.L., and Sossin, W.S. (2003). An activity-
1210 dependent switch to cap-independent translation triggered by eIF4E dephosphorylation. Nat
1211 Neurosci *6*, 219–220. https://doi.org/10.1038/nn1018.

1212 81. Chang, C., Music, N., Cheung, M., Rossignol, E., Bedi, S., Patel, H., Safari, M., Lee, C., Otten, G.R.,
1213 Settembre, E.C., et al. (2022). Self-amplifying mRNA bicistronic influenza vaccines raise cross-
1214 reactive immune responses in mice and prevent infection in ferrets. Molecular Therapy Methods &
1215 Clinical Development *27*, 195–205. https://doi.org/10.1016/j.omtm.2022.09.013.

1216 82. Koch, A., Aguilera, L., Morisaki, T., Munsky, B., and Stasevich, T.J. (2020). Quantifying the dynamics
1217 of IRES and cap translation with single-molecule resolution in live cells. Nat Struct Mol Biol *27*,
1218 1095–1104. https://doi.org/10.1038/s41594-020-0504-7.

1219 83. Ho, C.K., and Shuman, S. (1996). Physical and Functional Characterization of the Double-Stranded
1220 RNA Binding Protein Encoded by the Vaccinia Virus E3 Gene. Virology *217*, 272–284.
1221 https://doi.org/10.1006/viro.1996.0114.

1222 84. Dueck, K.J., Hu, Y. (Sandy), Chen, P., Deschambault, Y., Lee, J., Varga, J., and Cao, J. (2015).
1223 Mutational Analysis of Vaccinia Virus E3 Protein: the Biological Functions Do Not Correlate with Its
1224 Biochemical Capacity To Bind Double-Stranded RNA. Journal of Virology *89*, 5382–5394.
1225 https://doi.org/10.1128/jvi.03288-14.

1226 85. Leitner, W.W., Hwang, L.N., Bergmann-Leitner, E.S., Finkelstein, S.E., Frank, S., and Restifo, N.P.
1227 (2004). Apoptosis is essential for the increased efficacy of alphaviral replicase-based DNA vaccines.
1228 Vaccine *22*, 1537–1544. https://doi.org/10.1016/j.vaccine.2003.10.013.

1229 86. Wu, Y.-Y., Sun, T.-K., Chen, M.-S., Munir, M., and Liu, H.-J. (2023). Oncolytic viruses-modulated
1230 immunogenic cell death, apoptosis and autophagy linking to virotherapy and cancer immune
1231 response. Front. Cell. Infect. Microbiol. *13*. https://doi.org/10.3389/fcimb.2023.1142172.

1232 87. Li, Y., Banerjee, S., Wang, Y., Goldstein, S.A., Dong, B., Gaughan, C., Silverman, R.H., and Weiss, S.R.
1233 (2016). Activation of RNase L is dependent on OAS3 expression during infection with diverse human
1234 viruses. Proc Natl Acad Sci U S A *113*, 2241–2246. https://doi.org/10.1073/pnas.1519657113.

1235 88. Zuo, W., Wakimoto, M., Kozaiwa, N., Shirasaka, Y., Oh, S.-W., Fujiwara, S., Miyachi, H., Kogure, A.,
1236 Kato, H., and Fujita, T. (2022). PKR and TLR3 trigger distinct signals that coordinate the induction of
1237 antiviral apoptosis. Cell Death Dis *13*, 1–15. https://doi.org/10.1038/s41419-022-05101-3.

1238 89. Xu, C., Gamil, A.A.A., Munang'andu, H.M., and Evensen, Ø. (2018). Apoptosis Induction by dsRNA-
1239 Dependent Protein Kinase R (PKR) in EPC Cells via Caspase 8 and 9 Pathways. Viruses *10*, 526.
1240 https://doi.org/10.3390/v10100526.

1241 90. Gil, J., and Esteban, M. (2000). The interferon-induced protein kinase (PKR), triggers apoptosis
1242 through FADD-mediated activation of caspase 8 in a manner independent of Fas and TNF-α
1243 receptors. Oncogene *19*, 3665–3674. https://doi.org/10.1038/sj.onc.1203710.

1244 91. Zhang, P., and Samuel, C.E. (2007). Protein Kinase PKR Plays a Stimulus- and Virus-Dependent Role
1245 in Apoptotic Death and Virus Multiplication in Human Cells. Journal of Virology *81*, 8192–8200.
1246 https://doi.org/10.1128/jvi.00426-07.

1247 92. Roretz, C. von, and Gallouzi, I.-E. (2010). Protein Kinase RNA/FADD/Caspase-8 Pathway Mediates
1248 the Proapoptotic Activity of the RNA-binding Protein Human Antigen R (HuR). The Journal of
1249 Biological Chemistry *285*, 16806. https://doi.org/10.1074/jbc.M109.087320.

1250 93. Xi, J., Snieckute, G., Martínez, J.F., Arendrup, F.S.W., Asthana, A., Gaughan, C., Lund, A.H., Bekker-
1251 Jensen, S., and Silverman, R.H. (2024). Initiation of a ZAKα-dependent ribotoxic stress response by
1252 the innate immunity endoribonuclease RNase L. Cell Reports *43*.
1253 https://doi.org/10.1016/j.celrep.2024.113998.

1254 94. Guydosh, N.R., Kimmig, P., Walter, P., and Green, R. (2017). Regulated Ire1-dependent mRNA decay
1255 requires no-go mRNA degradation to maintain endoplasmic reticulum homeostasis in S. pombe.
1256 eLife *6*, e29216. https://doi.org/10.7554/eLife.29216.

1257 95. Snieckute, G., Genzor, A.V., Vind, A.C., Ryder, L., Stoneley, M., Chamois, S., Dreos, R., Nordgaard, C.,
1258 Sass, F., Blasius, M., et al. (2022). Ribosome stalling is a signal for metabolic regulation by the
1259 ribotoxic stress response. Cell Metab *34*, 2036-2046.e8.
1260 https://doi.org/10.1016/j.cmet.2022.10.011.

1261 96. Li, G., Xiang, Y., Sabapathy, K., and Silverman, R.H. (2004). An Apoptotic Signaling Pathway in the
1262 Interferon Antiviral Response Mediated by RNase L and c-Jun NH2-terminal Kinase *. Journal of
1263 Biological Chemistry *279*, 1123–1131. https://doi.org/10.1074/jbc.M305893200.

1264 97. Samuel, C.E., Kuhen, K.L., George, C.X., Ortega, L.G., Rende-Fournier, R., and Tanaka, H. (1997). The
1265 PKR protein kinase--an interferon-inducible regulator of cell growth and differentiation. Int J
1266 Hematol *65*, 227–237. https://doi.org/10.1016/s0925-5710(96)00544-0.

1267 98. Iordanov, M.S., Wong, J., Bell, J.C., and Magun, B.E. (2001). Activation of NF-κB by Double-Stranded
1268 RNA (dsRNA) in the Absence of Protein Kinase R and RNase L Demonstrates the Existence of Two
1269 Separate dsRNA-Triggered Antiviral Programs. Molecular and Cellular Biology *21*, 61–72.
1270 https://doi.org/10.1128/MCB.21.1.61-72.2001.

1271 99. Herdy, B., Jaramillo, M., Svitkin, Y.V., Rosenfeld, A.B., Kobayashi, M., Walsh, D., Alain, T., Sean, P.,
1272 Robichaud, N., Topisirovic, I., et al. (2012). Translational control of the activation of transcription
1273 factor NF-κB and production of type I interferon by phosphorylation of the translation factor eIF4E.
1274 Nat Immunol *13*, 543–550. https://doi.org/10.1038/ni.2291.

1275 100. Liu, T., Zhang, L., Joo, D., and Sun, S.-C. (2017). NF-κB signaling in inflammation. Sig Transduct
1276 Target Ther *2*, 1–9. https://doi.org/10.1038/sigtrans.2017.23.

1277 101. Luo, J.-L., Kamata, H., and Karin, M. (2005). IKK/NF-κB signaling: balancing life and death – a new
1278 approach to cancer therapy. Journal of Clinical Investigation *115*, 2625–2632.
1279 https://doi.org/10.1172/JCI26322.

1280 102. Miagkov, A.V., Kovalenko, D.V., Brown, C.E., Didsbury, J.R., Cogswell, J.P., Stimpson, S.A.,
1281 Baldwin, A.S., and Makarov, S.S. (1998). NF-κB activation provides the potential link between
1282 inflammation and hyperplasia in the arthritic joint. Proceedings of the National Academy of Sciences
1283 *95*, 13859–13864. https://doi.org/10.1073/pnas.95.23.13859.

1284 103. Zhang, H.G., Huang, N., Liu, D., Bilbao, L., Zhang, X., Yang, P., Zhou, T., Curiel, D.T., and Mountz,
1285 J.D. (2000). Gene therapy that inhibits nuclear translocation of nuclear factor kappaB results in
1286 tumor necrosis factor alpha-induced apoptosis of human synovial fibroblasts. Arthritis Rheum *43*,
1287 1094–1105. https://doi.org/10.1002/1529-0131(200005)43:5<1094::AID-ANR20>3.0.CO;2-V.

1288 104. Xu, Y., Bialik, S., Jones, B.E., Iimuro, Y., Kitsis, R.N., Srinivasan, A., Brenner, D.A., and Czaja, M.J.
1289 (1998). NF-kappaB inactivation converts a hepatocyte cell line TNF-alpha response from
1290 proliferation to apoptosis. Am J Physiol *275*, C1058-1066.
1291 https://doi.org/10.1152/ajpcell.1998.275.4.C1058.

1292 105. Sago, C.D., Krupczak, B.R., Lokugamage, M.P., Gan, Z., and Dahlman, J.E. (2019). Cell Subtypes
1293 Within the Liver Microenvironment Differentially Interact with Lipid Nanoparticles. Cellular and
1294 Molecular Bioengineering *12*, 389. https://doi.org/10.1007/s12195-019-00573-4.

1295 106. Yamamura, Y., Hua, X., Bergelson, S., and Lodish, H.F. (2000). Critical Role of Smads and AP-1
1296 Complex in Transforming Growth Factor-β-dependent Apoptosis. Journal of Biological Chemistry
1297 *275*, 36295–36302. https://doi.org/10.1074/jbc.M006023200.

1298 107. Patil, S., Wildey, G.M., Brown, T.L., Choy, L., Derynck, R., and Howe, P.H. (2000). Smad7 is
1299 induced by CD40 and protects WEHI 231 B-lymphocytes from transforming growth factor-beta -
1300 induced growth inhibition and apoptosis. J Biol Chem *275*, 38363–38370.
1301 https://doi.org/10.1074/jbc.M004861200.

1302 108. Zitzmann, K., Brand, S., De Toni, E.N., Baehs, S., Göke, B., Meinecke, J., Spöttl, G., Meyer,
1303 H.H.H.D., and Auernhammer, C.J. (2007). SOCS1 Silencing Enhances Antitumor Activity of Type I IFNs
1304 by Regulating Apoptosis in Neuroendocrine Tumor Cells. Cancer Research *67*, 5025–5032.
1305 https://doi.org/10.1158/0008-5472.CAN-06-2575.

1306 109. Mann-Chandler, M.N., Kashyap, M., Wright, H.V., Norozian, F., Barnstein, B.O., Gingras, S.,
1307 Parganas, E., and Ryan, J.J. (2005). IFN-γ Induces Apoptosis in Developing Mast Cells1. The Journal of
1308 Immunology *175*, 3000–3005. https://doi.org/10.4049/jimmunol.175.5.3000.

1309 110. Kimura, A., Naka, T., Nagata, S., Kawase, I., and Kishimoto, T. (2004). SOCS-1 suppresses TNF-
1310 alpha-induced apoptosis through the regulation of Jak activation. Int Immunol *16*, 991–999.
1311 https://doi.org/10.1093/intimm/dxh102.

1312 111. Madonna, S., Scarponi, C., Pallotta, S., Cavani, A., and Albanesi, C. (2012). Anti-apoptotic effects
1313 of suppressor of cytokine signaling 3 and 1 in psoriasis. Cell Death Dis *3*, e334–e334.
1314 https://doi.org/10.1038/cddis.2012.69.

1315 112. Yan, L., Tang, Q., Shen, D., Peng, S., Zheng, Q., Guo, H., Jiang, M., and Deng, W. (2008). SOCS-1
1316 Inhibits TNF-α-Induced Cardiomyocyte Apoptosis via ERK1/2 Pathway Activation. Inflammation *31*,
1317 180–188. https://doi.org/10.1007/s10753-008-9063-5.

1318 113. Goker Bagca, B., and Biray Avci, C. (2020). The potential of JAK/STAT pathway inhibition by
1319 ruxolitinib in the treatment of COVID-19. Cytokine & Growth Factor Reviews *54*, 51–61.
1320 https://doi.org/10.1016/j.cytogfr.2020.06.013.

1321 114. Liau, N.P.D., Laktyushin, A., Lucet, I.S., Murphy, J.M., Yao, S., Whitlock, E., Callaghan, K., Nicola,
1322 N.A., Kershaw, N.J., and Babon, J.J. (2018). The molecular basis of JAK/STAT inhibition by SOCS1. Nat
1323 Commun *9*, 1558. https://doi.org/10.1038/s41467-018-04013-1.

1324 115. Skidmore, A.M., Adcock, R.S., Jonsson, C.B., Golden, J.E., and Chung, D.-H. (2020). Benzamidine
1325 ML336 inhibits plus and minus strand RNA synthesis of Venezuelan equine encephalitis virus
1326 without affecting host RNA production. Antiviral Research *174*, 104674.
1327 https://doi.org/10.1016/j.antiviral.2019.104674.

1328 116. Schroeder, C.E., Yao, T., Sotsky, J., Smith, R.A., Roy, S., Chu, Y.-K., Guo, H., Tower, N.A., Noah,
1329 J.W., McKellip, S., et al. (2014). Development of (E)-2-((1,4-Dimethylpiperazin-2-ylidene)amino)-5-
1330 nitro-N-phenylbenzamide, ML336: Novel 2-Amidinophenylbenzamides as Potent Inhibitors of
1331 Venezuelan Equine Encephalitis Virus. J. Med. Chem. *57*, 8608–8621.
1332 https://doi.org/10.1021/jm501203v.

1333 117. Tregoning, J.S., Stirling, D.C., Wang, Z., Flight, K.E., Brown, J.C., Blakney, A.K., McKay, P.F.,
1334 Cunliffe, R.F., Murugaiah, V., Fox, C.B., et al. (2023). Formulation, inflammation, and RNA sensing
1335 impact the immunogenicity of self-amplifying RNA vaccines. Molecular Therapy Nucleic Acids *31*,
1336 29–42. https://doi.org/10.1016/j.omtn.2022.11.024.

1337 118. Bathula, N.V., Friesen, J.J., Casmil, I.C., Wayne, C.J., Liao, S., Soriano, S.K.V., Ho, C.H., Strumpel,
1338 A., and Blakney, A.K. (2024). Delivery vehicle and route of administration influences self-amplifying
1339 RNA biodistribution, expression kinetics, and reactogenicity. Journal of Controlled Release *374*, 28–
1340 38. https://doi.org/10.1016/j.jconrel.2024.07.078.

1341 119. Oda, Y., Kumagai, Y., Kanai, M., Iwama, Y., Okura, I., Minamida, T., Yagi, Y., Kurosawa, T.,
1342 Greener, B., Zhang, Y., et al. (2024). Immunogenicity and safety of a booster dose of a self-
1343 amplifying RNA COVID-19 vaccine (ARCT-154) versus BNT162b2 mRNA COVID-19 vaccine: a double-
1344 blind, multicentre, randomised, controlled, phase 3, non-inferiority trial. The Lancet Infectious
1345 Diseases *24*, 351–360. https://doi.org/10.1016/S1473-3099(23)00650-3.

1346 120. Saraf, A., Gurjar, R., Kaviraj, S., Kulkarni, A., Kumar, D., Kulkarni, R., Virkar, R., Krishnan, J., Yadav,
1347 A., Baranwal, E., et al. (2024). An Omicron-specific, self-amplifying mRNA booster vaccine for COVID-
1348 19: a phase 2/3 randomized trial. Nat Med *30*, 1363–1372. https://doi.org/10.1038/s41591-024-
1349 02955-2.

1350 121. Roman-Blas, J.A., and Jimenez, S.A. (2006). NF-κB as a potential therapeutic target in
1351 osteoarthritis and rheumatoid arthritis. Osteoarthritis and Cartilage *14*, 839–848.
1352 https://doi.org/10.1016/j.joca.2006.04.008.

1353 122. Shen, J., Li, S., and Chen, D. (2014). TGF-β signaling and the development of osteoarthritis. Bone
1354 Res *2*, 1–7. https://doi.org/10.1038/boneres.2014.2.

1355 123. Zhou, Q., Ren, Q., Jiao, L., Huang, J., Yi, J., Chen, J., Lai, J., Ji, G., and Zheng, T. (2022). The
1356 potential roles of JAK/STAT signaling in the progression of osteoarthritis. Front. Endocrinol. *13*.
1357 https://doi.org/10.3389/fendo.2022.1069057.

1358 124. Blackwell, N.M., Sembi, P., Newson, J.S., Lawrence, T., Gilroy, D.W., and Kabouridis, P.S. (2004).
1359 Reduced infiltration and increased apoptosis of leukocytes at sites of inflammation by systemic
1360 administration of a membrane-permeable IκBα repressor. Arthritis & Rheumatism *50*, 2675–2684.
1361 https://doi.org/10.1002/art.20467.

1362 125. Chen, S.-Y., Shiau, A.-L., Wu, C.-L., and Wang, C.-R. (2016). Intraarticular overexpression of
1363 Smad7 ameliorates experimental arthritis. Sci Rep *6*, 35163. https://doi.org/10.1038/srep35163.

1364 126. Ha, Y.-J., Choi, Y.S., Kang, E.H., Shin, K., Kim, T.K., Song, Y.W., and Lee, Y.J. (2016). SOCS1
1365 suppresses IL-1β-induced C/EBPβ expression via transcriptional regulation in human chondrocytes.
1366 Exp Mol Med *48*, e241–e241. https://doi.org/10.1038/emm.2016.47.

1367 127. Freppel, W., Lim, E.X.Y., Rudd, P.A., and Herrero, L.J. (2024). Synoviocytes assist in modulating
1368 the effect of Ross River virus infection in micromass-cultured primary human chondrocytes. J Med
1369 Microbiol *73*, 001859. https://doi.org/10.1099/jmm.0.001859.

1370 128. Legros, V., Belarbi, E., Jeannin, P., Kümmerer, B., Hardy, D., Desprès, P., Gessain, A., Roques, P.,
1371 Ceccaldi, P.-E., and Choumet, V. (2024). A recombinant CHIKV-NLuc virus identifies chondrocytes as
1372 target of Chikungunya virus in a immunocompetent mouse model. Preprint at bioRxiv,
1373 https://doi.org/10.1101/2024.05.20.594924 https://doi.org/10.1101/2024.05.20.594924.

1374 129. Wäldele, S., Koers-Wunrau, C., Beckmann, D., Korb-Pap, A., Wehmeyer, C., Pap, T., and Dankbar,
1375 B. (2015). Deficiency of fibroblast activation protein alpha ameliorates cartilage destruction in
1376 inflammatory destructive arthritis. Arthritis Res Ther *17*, 12. https://doi.org/10.1186/s13075-015-
1377 0524-6.

1378 130. Petrakova, O., Volkova, E., Gorchakov, R., Paessler, S., Kinney, R.M., and Frolov, I. (2005).
1379 Noncytopathic Replication of Venezuelan Equine Encephalitis Virus and Eastern Equine Encephalitis
1380 Virus Replicons in Mammalian Cells. J Virol *79*, 7597–7608. https://doi.org/10.1128/JVI.79.12.7597-
1381 7608.2005.

1382 131. Hariri, F., Arguello, M., Volpon, L., Culjkovic-Kraljacic, B., Nielsen, T.H., Hiscott, J., Mann, K.K.,
1383 and Borden, K.L.B. (2013). The eukaryotic translation initiation factor eIF4E is a direct transcriptional
1384 target of NF-κB and is aberrantly regulated in acute myeloid leukemia. Leukemia *27*, 2047–2055.
1385 https://doi.org/10.1038/leu.2013.73.

1386 132. Uttam, S., Wong, C., Price, T.J., and Khoutorsky, A. (2018). eIF4E-Dependent Translational
1387 Control: A Central Mechanism for Regulation of Pain Plasticity. Front Genet *9*, 470.
1388 https://doi.org/10.3389/fgene.2018.00470.

1389 133. Siddiqui, N., and Sonenberg, N. (2015). Signalling to eIF4E in cancer. Biochemical Society
1390 Transactions *43*, 763–772. https://doi.org/10.1042/BST20150126.

1391 134. Gkogkas, C.G., Khoutorsky, A., Ran, I., Rampakakis, E., Nevarko, T., Weatherill, D.B., Vasuta, C.,
1392 Yee, S., Truitt, M., Dallaire, P., et al. (2013). Autism-related deficits via dysregulated eIF4E-
1393 dependent translational control. Nature *493*, 371–377. https://doi.org/10.1038/nature11628.

1394 135. Syntichaki, P., Troulinaki, K., and Tavernarakis, N. (2007). eIF4E function in somatic cells
1395 modulates ageing in Caenorhabditis elegans. Nature *445*, 922–926.
1396 https://doi.org/10.1038/nature05603.

1397 136. Costa-Mattioli, M., and Walter, P. (2020). The integrated stress response: From mechanism to
1398 disease. Science *368*, eaat5314. https://doi.org/10.1126/science.aat5314.

1399 137. Hồ, N.T., Hughes, S.G., Ta, V.T., Phan, L.T., Đỗ, Q., Nguyễn, T.V., Phạm, A.T.V., Thị Ngọc Đặng, M.,
1400 Nguyễn, L.V., Trịnh, Q.V., et al. (2024). Safety, immunogenicity and efficacy of the self-amplifying
1401 mRNA ARCT-154 COVID-19 vaccine: pooled phase 1, 2, 3a and 3b randomized, controlled trials. Nat
1402 Commun *15*, 4081. https://doi.org/10.1038/s41467-024-47905-1.

1403 138. Gadella, T.W.J., van Weeren, L., Stouthamer, J., Hink, M.A., Wolters, A.H.G., Giepmans, B.N.G.,
1404 Aumonier, S., Dupuy, J., and Royant, A. (2023). mScarlet3: a brilliant and fast-maturing red
1405 fluorescent protein. Nat Methods *20*, 541–545. https://doi.org/10.1038/s41592-023-01809-y.

1406 139. Costantini, L.M., Baloban, M., Markwardt, M.L., Rizzo, M.A., Guo, F., Verkhusha, V.V., and Snapp,
1407 E.L. (2015). A palette of fluorescent proteins optimized for diverse cellular environments. Nat
1408 Commun *6*, 7670. https://doi.org/10.1038/ncomms8670.

1409 140. Chakrabarti, S., Hore, Z., Pattison, L.A., Lalnunhlimi, S., Bhebhe, C.N., Callejo, G., Bulmer, D.C.,
1410 Taams, L.S., Denk, F., and Smith, E.S.J. (2020). Sensitization of knee-innervating sensory neurons by
1411 tumor necrosis factor-α-activated fibroblast-like synoviocytes: an in vitro, coculture model of
1412 inflammatory pain. Pain *161*, 2129–2141. https://doi.org/10.1097/j.pain.0000000000001890.

1413 141. Li, C.H., and Lee, C.K. (1993). Minimum cross entropy thresholding. Pattern Recognition *26*, 617–
1414 625. https://doi.org/10.1016/0031-3203(93)90115-D.

1415

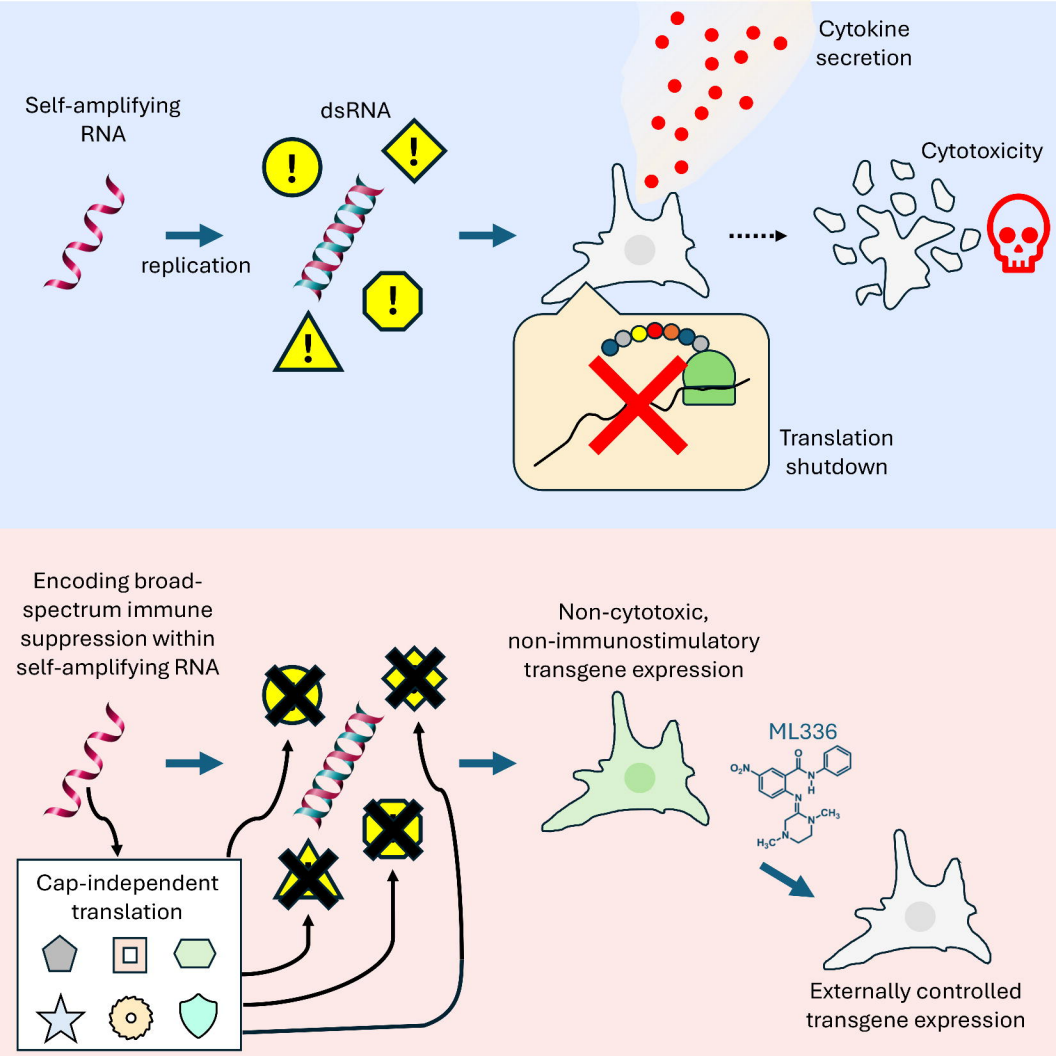
Self-amplifying RNA
replication
dsRNA
Cytokine secretion
Cytotoxicity
Translation shutdown
Encoding broad-spectrum immune suppression within self-amplifying RNA
Cap-independent translation
Non-cytotoxic, non-immunostimulatory transgene expression
ML336
Externally controlled transgene expression

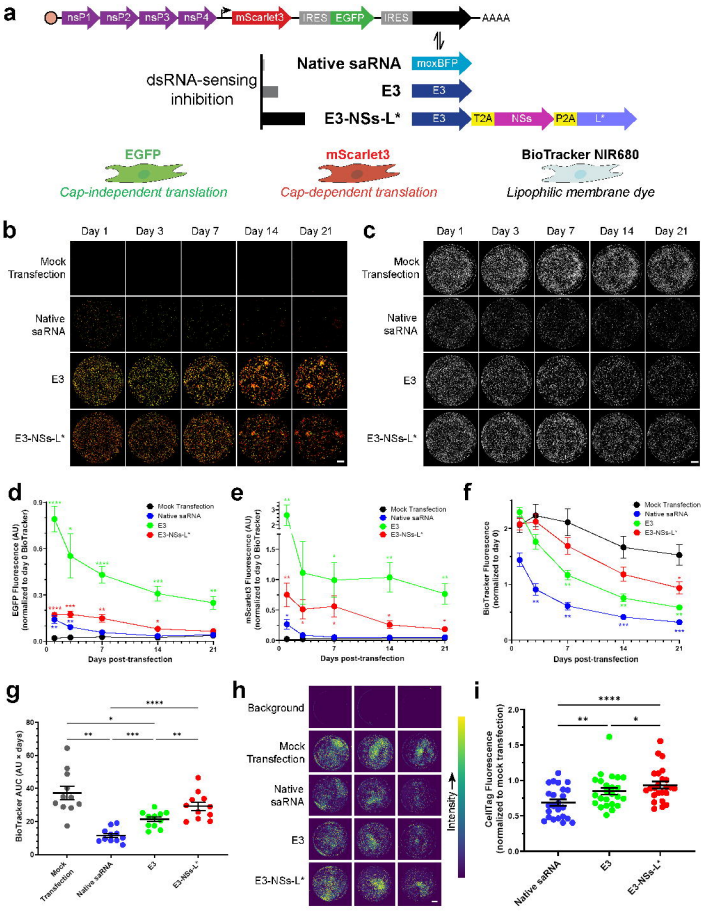
a
nsP1
nsP2
nsP3
nsP4
mScarlet3
IRES
EGFP
IRES
AAAA
dsRNA-sensing inhibition
Native saRNA
mcxBFP
E3
E3
E3-NSs-L*
E3
T2A
NSs
P2A
L*
EGFP
Cap-independent translation
mScarlet3
Cap-dependent translation
BioTracker NIR680
Lipophilic membrane dye
b
Day 1
Day 3
Day 7
Day 14
Day 21
Mock Transfection
Native saRNA
E3
E3-NSs-L*
c
Day 1
Day 3
Day 7
Day 14
Day 21
Mock Transfection
Native saRNA
E3
E3-NSs-L*
d
Mock Transfection
Native saRNA
E3
E3-NSs-L*
EGFP Fluorescence (AU)
(normalized to day 0 BioTracker)
Days post-transfection
e
Mock Transfection
Native saRNA
E3
E3-NSs-L*
mScarlet3 Fluorescence (AU)
(normalized to day 0 BioTracker)
Days post-transfection
f
Mock Transfection
Native saRNA
E3
E3-NSs-L*
BioTracker Fluorescence
(normalized to day 0)
Days post-transfection
g
BioTracker AUC (AU × days)
Mock Transfection
Native saRNA
E3
E3-NSs-L*
h
Background
Mock Transfection
Native saRNA
E3
E3-NSs-L*
Intensity
i
CellTag Fluorescence
(normalized to mock transfection)
Native saRNA
E3
E3-NSs-L*

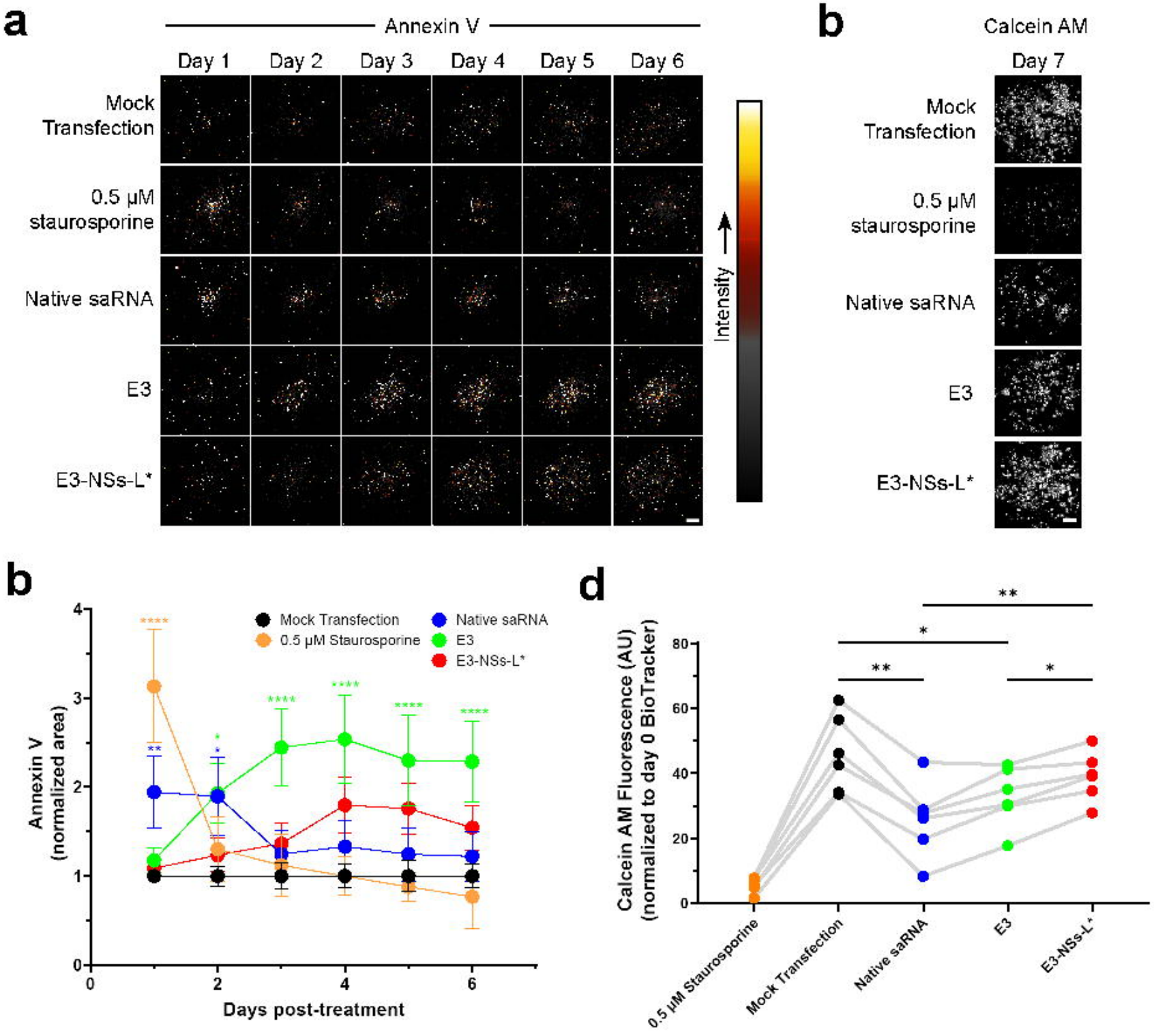
a
Annexin V
Day 1
Day 2
Day 3
Day 4
Day 5
Day 6
Mock Transfection
0.5 μM staurosporine
Native saRNA
E3
E3-NSs-L*
Intensity
b
Calcein AM
Day 7
Mock Transfection
0.5 μM staurosporine
Native saRNA
E3
E3-NSs-L*
b
Mock Transfection
0.5 μM Staurosporine
Native saRNA
E3
E3-NSs-L*
Annexin V (normalized area)
Days post-treatment
d
Calcein AM Fluorescence (AU) (normalized to day 0 BioTracker)
0.5 μM Staurosporine
Mock Transfection
Native saRNA
E3
E3-NSs-L*

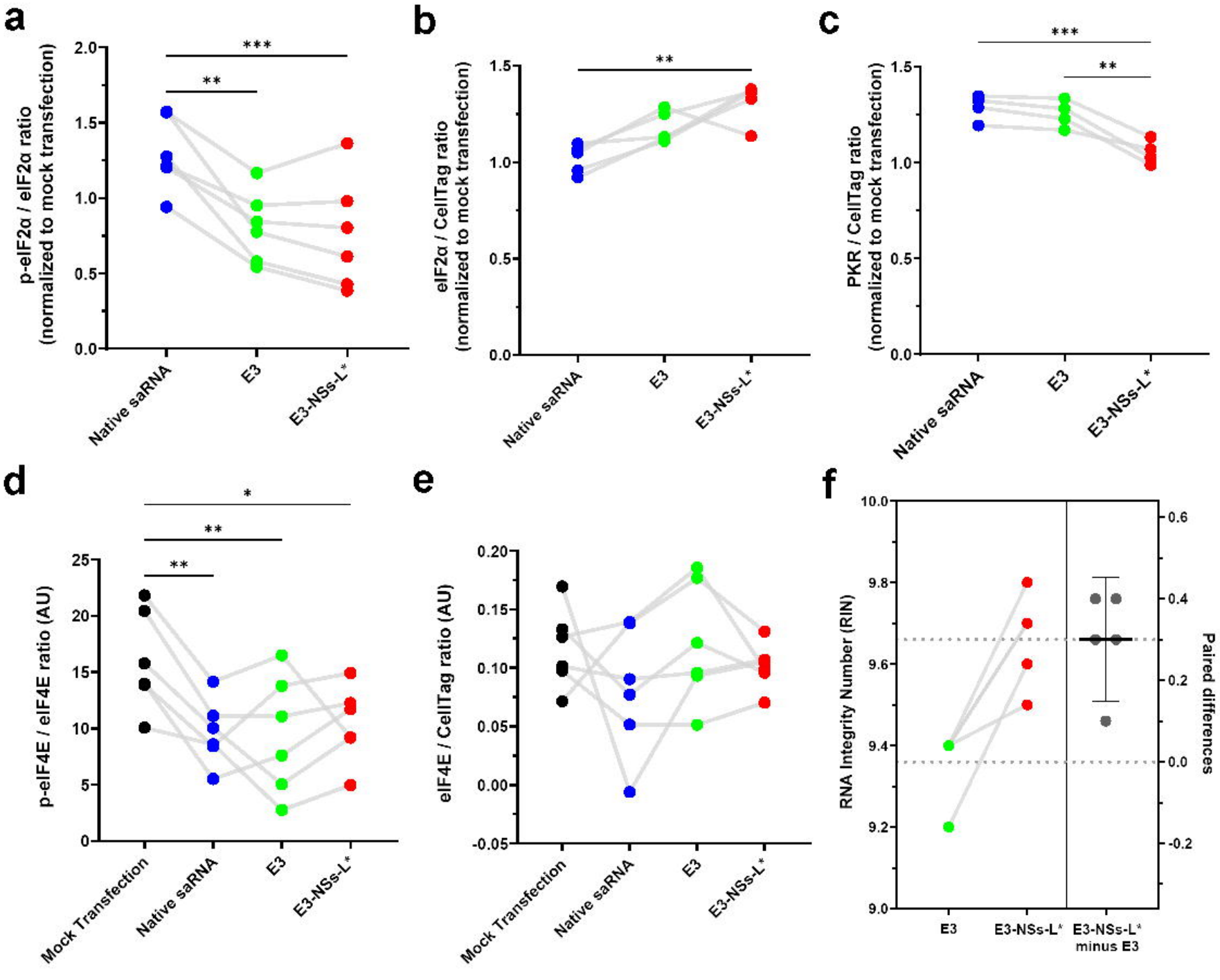
a
p-eIF2α / eIF2α ratio
(normalized to mock transfection)
2.0
1.5
1.0
0.5
0.0
***
**
Native saRNA
E3
E3-NSs-L*
b
eIF2α / CellTag ratio
(normalized to mock transfection)
1.5
1.0
0.5
0.0
**
Native saRNA
E3
E3-NSs-L*
c
PKR / CellTag ratio
(normalized to mock transfection)
1.5
1.0
0.5
0.0
***
**
Native saRNA
E3
E3-NSs-L*
d
p-eIF4E / eIF4E ratio (AU)
25
20
15
10
5
0
*
**
**
Mock Transfection
Native saRNA
E3
E3-NSs-L*
e
eIF4E / CellTag ratio (AU)
0.20
0.15
0.10
0.05
0.00
-0.05
Mock Transfection
Native saRNA
E3
E3-NSs-L*
f
RNA Integrity Number (RIN)
10.0
9.8
9.6
9.4
9.2
9.0
Paired differences
0.6
0.4
0.2
0.0
-0.2
E3
E3-NSs-L*
E3-NSs-L*
minus E3

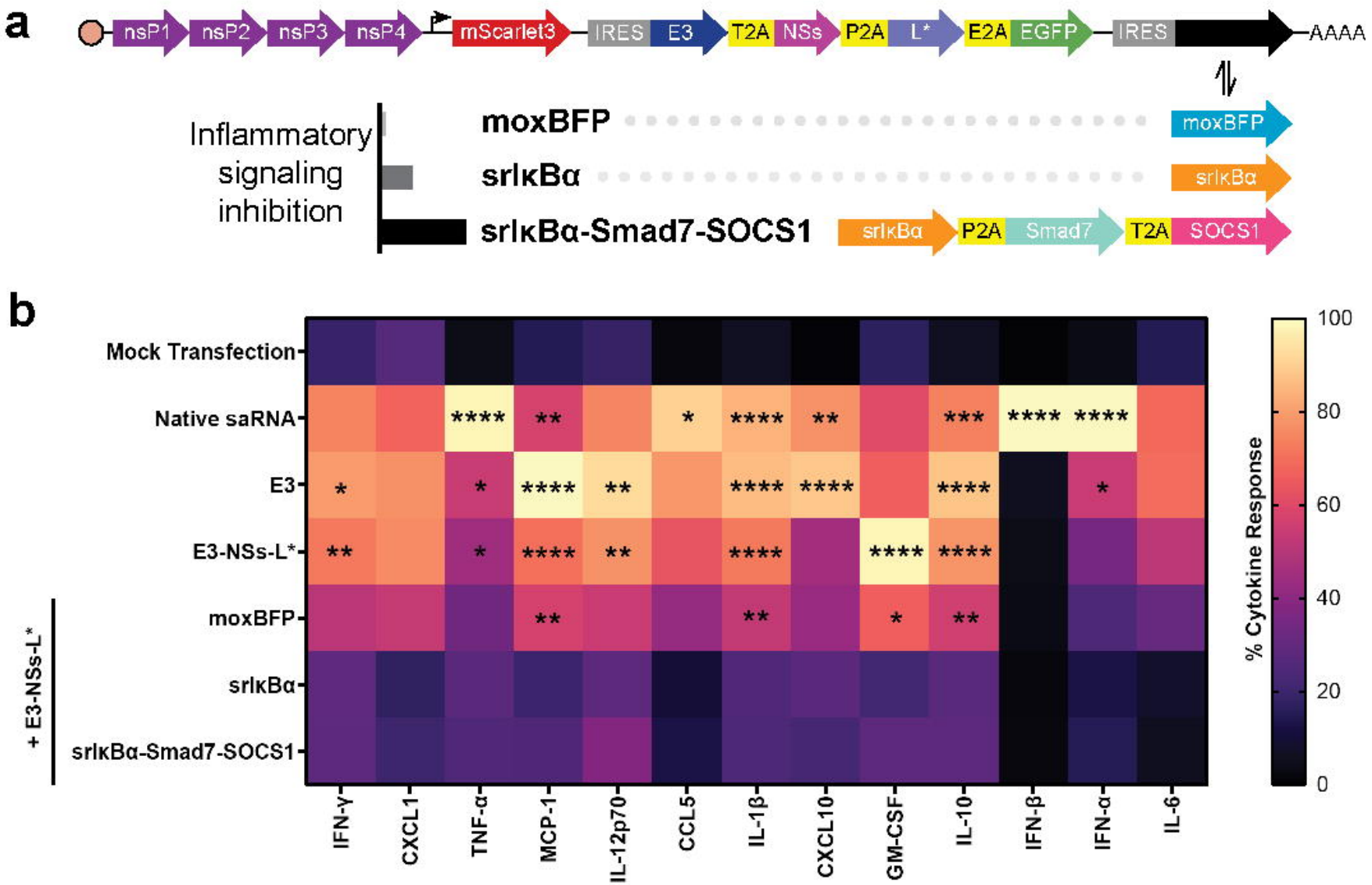
a
nsP1
nsP2
nsP3
nsP4
mScarlet3
IRES
E3
T2A
NSs
P2A
L*
E2A
EGFP
IRES
AAAA
Inflammatory signaling inhibition
moxBFP
srIκBα
srIκBα-Smad7-SOCS1
moxBFP
srIκBα
srIκBα
P2A
Smad7
T2A
SOCS1
b
Mock Transfection
Native saRNA
E3
E3-NSs-L*
moxBFP
srIκBα
srIκBα-Smad7-SOCS1
+ E3-NSs-L*
IFN-γ
CXCL1
TNF-α
MCP-1
IL-12p70
CCL5
IL-1β
CXCL10
GM-CSF
IL-10
IFN-β
IFN-α
IL-6
% Cytokine Response
100
80
60
40
20
0

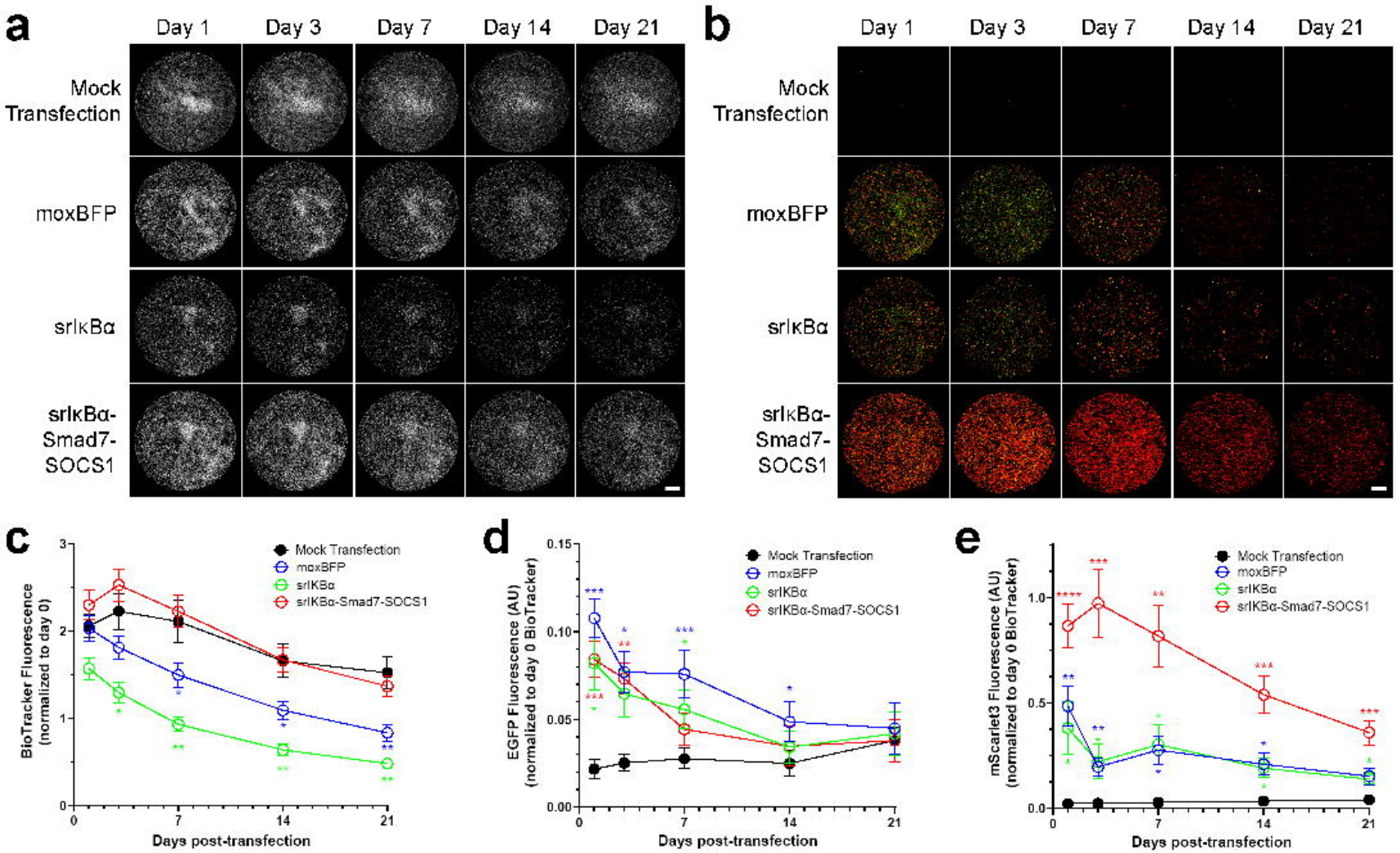
a
Day 1
Day 3
Day 7
Day 14
Day 21
Mock Transfection
moxBFP
srIκBα
srIκBα-Smad7-SOCS1
b
Day 1
Day 3
Day 7
Day 14
Day 21
Mock Transfection
moxBFP
srIκBα
srIκBα-Smad7-SOCS1
c
BioTracker Fluorescence (normalized to day 0)
Days post-transfection
Mock Transfection
moxBFP
srIKBα
srIKBα-Smad7-SOCS1
d
EGFP Fluorescence (AU) (normalized to day 0 BioTracker)
Days post-transfection
Mock Transfection
moxBFP
srIKBα
srIKBα-Smad7-SOCS1
e
mScarlet3 Fluorescence (AU) (normalized to day 0 BioTracker)
Days post-transfection
Mock Transfection
moxBFP
srIKBα
srIKBα-Smad7-SOCS1

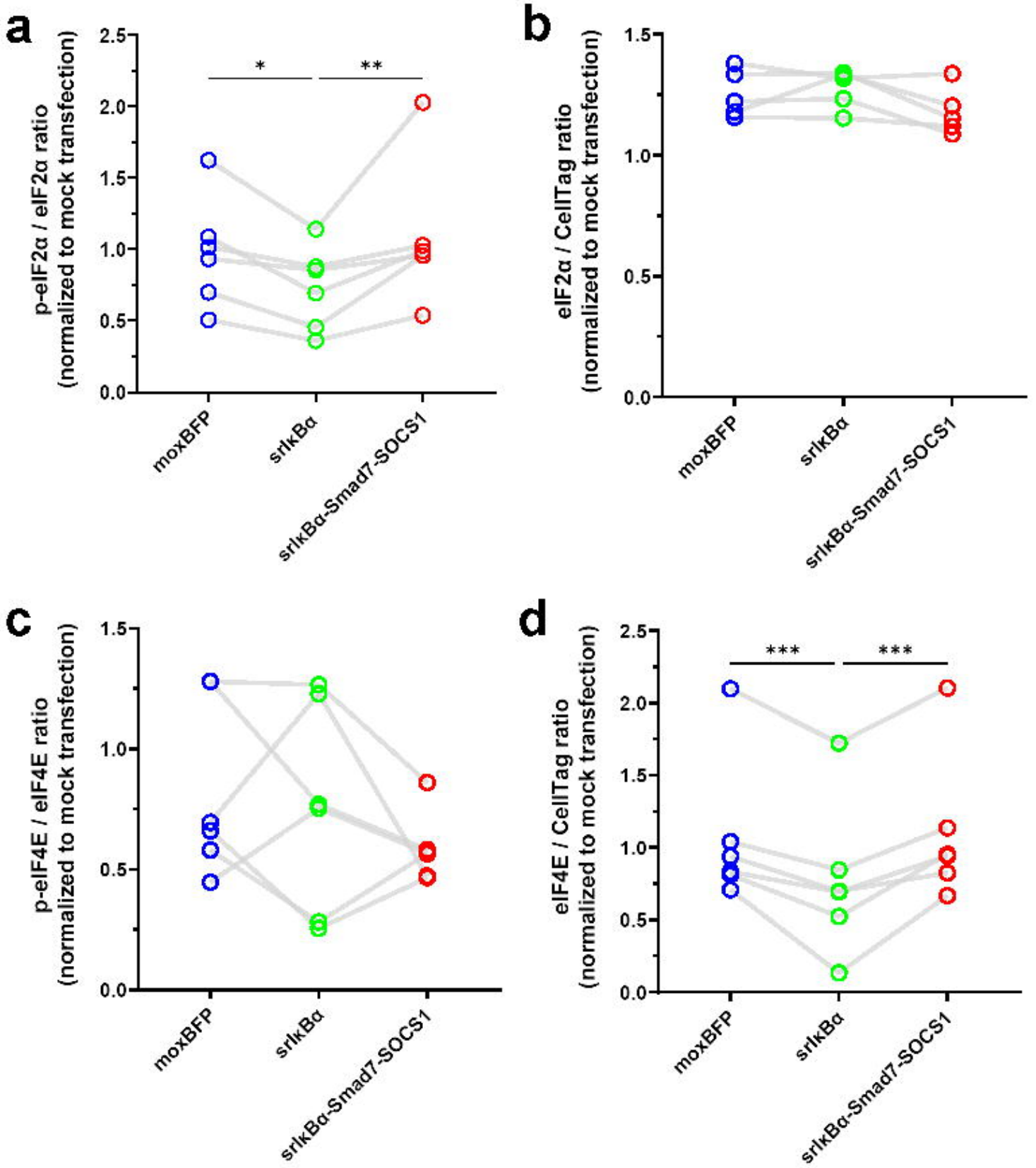
a
p-eIF2α / eIF2α ratio
(normalized to mock transfection)
2.5
2.0
1.5
1.0
0.5
0.0
*
**
moxBFP
srIκBα
srIκBα-Smad7-SOCS1
b
eIF2α / CellTag ratio
(normalized to mock transfection)
1.5
1.0
0.5
0.0
moxBFP
srIκBα
srIκBα-Smad7-SOCS1
c
p-eIF4E / eIF4E ratio
(normalized to mock transfection)
1.5
1.0
0.5
0.0
moxBFP
srIκBα
srIκBα-Smad7-SOCS1
d
eIF4E / CellTag ratio
(normalized to mock transfection)
2.5
2.0
1.5
1.0
0.5
0.0
***
***
moxBFP
srIκBα
srIκBα-Smad7-SOCS1

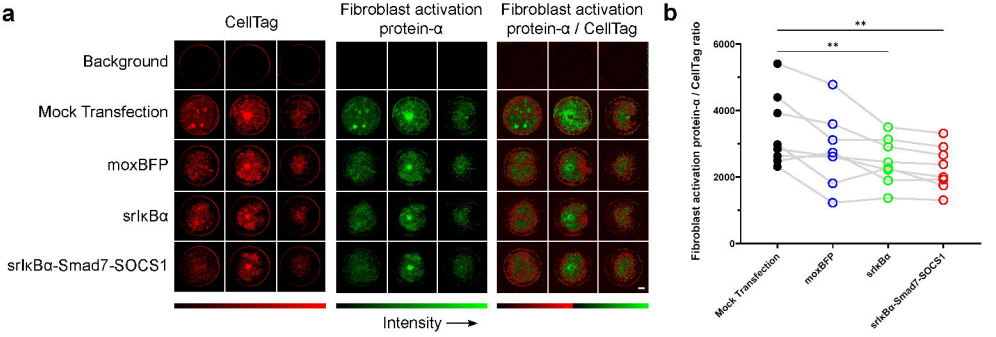
a
CellTag
Fibroblast activation protein-α
Fibroblast activation protein-α / CellTag
Background
Mock Transfection
moxBFP
srIκBα
srIκBα-Smad7-SOCS1
Intensity
b
Fibroblast activation protein-α / CellTag ratio
6000
4000
2000
0
**
**
Mock Transfection
moxBFP
srIκBα
srIκBα-Smad7-SOCS1

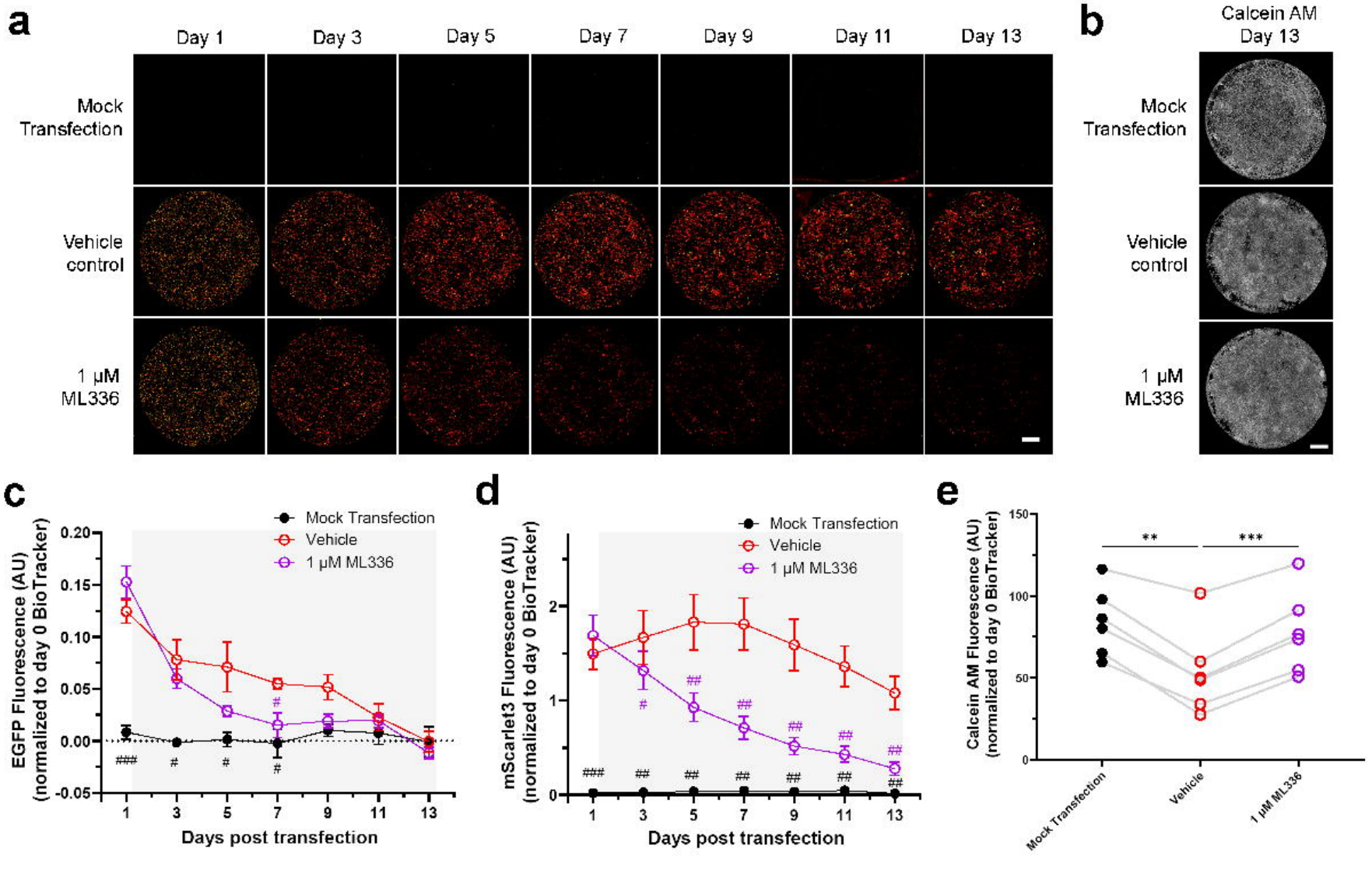
a
Day 1
Day 3
Day 5
Day 7
Day 9
Day 11
Day 13
Mock Transfection
Vehicle control
1 μM ML336
b
Calcein AM Day 13
Mock Transfection
Vehicle control
1 μM ML336
c
Mock Transfection
Vehicle
1 μM ML336
EGFP Fluorescence (AU) (normalized to day 0 BioTracker)
Days post transfection
d
Mock Transfection
Vehicle
1 μM ML336
mScarlet3 Fluorescence (AU) (normalized to day 0 BioTracker)
Days post transfection
e
Calcein AM Fluorescence (AU) (normalized to day 0 BioTracker)
Mock Transfection
Vehicle
1 μM ML336